EBERHARD *et al.*

Thus we see that there is no obvious resonance in the s channel indicated by our data, and that simple exchange models in the t and u channels do not fit the data. We have not yet embarked upon an investigation of the absorption model.[8]

---

[8] J. D. Jackson, Rev. Mod. Phys. **37**, 484 (1965).

ACKNOWLEDGMENTS

Nonstrange-Resonance Production in π^+p Collisions at 2.35, 2.62, and 2.90 BeV/c*

C. Alff-Steinberger,† D. Berley,‡ D. Colley,§ N. Gelfand,‖ D. Miller,** U. Nauenberg,††
J. Schultz,‡‡ AND T. H. Tan§§

Columbia University, New York, New York

AND

H. Brugger,‖‖ P. Kramer,*** AND R. Plano

Rutgers, The State University, New Brunswick, New Jersey

(Received 2 December 1965)

In an exposure of the Brookhaven National Laboratory 20-in. hydrogen bubble chamber to a separated π^+ beam at π^+ momenta of 2.35 BeV/c (center-of-mass energy $E^* = 2.30$ BeV), 2.62 BeV/c ($E^* = 2.41$ BeV), and 2.90 BeV/c ($E^* = 2.52$ BeV), we have observed production of the ω^0, ρ^0, and η^0 mesons. The production of the ω^0, ρ^0, and η^0 is often accompanied by simultaneous production of the N^{*++}. The momentum transfer in ω^0 and ρ^0 production is characteristic of peripheral collisions and suggests a single-particle exchange for the production mechanism. The decay distributions for the ω^0, ρ^0, and the ρ^+ demonstrate the importance of modifying the single-particle-exchange model to include absorptive effects. An upper limit on the two-π decay of the ω^0 is set at 2%. The width of the η^0 is found to be less than 10 MeV. Elastic-scattering distributions are presented.

I. INTRODUCTION

WE have[1] exposed the Brookhaven National Laboratory 20-in.[2] liquid-hydrogen bubble chamber to a separated π^+ beam.[3] The π^+ beam momenta were 2.35, 2.62, and 2.90 BeV/c.[4] The pictures were scanned for two- and four-pronged events originating within a restricted fiducial volume. Additional criteria were imposed to ensure that the measured momenta were significant. The events were measured on film plane digitizers. The geometric reconstruction for the events was done on an IBM 7090 using the Nevis Laboratories NP-54 program.[5] Kinematic fitting was done using the UCRL GUTS subroutine.[6]

---

[1] A report on the preliminary results of this experiment may be found in C. Alff *et al.*, Phys. Rev. Letters **9**, 322 (1962) and C. Alff *et al.*, *ibid.* **9**, 325 (1962). Further details can be found in T. H. Tan, Nevis Report 123 (unpublished); N. Gelfand, Nevis Report 137 (unpublished).
[2] R. I. Louttit, in *Proceedings of an International Conference on Instrumentation for High Energy Physics* (Interscience Publishers, Inc., New York, 1961).
[3] C. Baltay, thesis presented to Yale University, 1963 (un-published); C. Baltay, J. Sandweiss, J. Sanford, H. Brown, M. Webster, and S. Yamamoto, Nucl. Instr. Methods **20**, 37 (1963).
[4] The results of other π^+p experiments in the energy region above 2 BeV/c may be found in: N. H. Xuong, R. L. Lander, W. A. Mehlhop, and P. M. Yeager, Phys. Rev. Letters **11**, 227 (1963). G. Goldhaber, J. L. Brown, S. Goldhaber, J. A. Kadyk, B. C. Shen, and G. H. Trilling, *ibid.* **12**, 336 (1964). Aachen, Berlin, Birmingham, Bonn, Hamburg, London (I.C.), München collaboration reported in Nuovo Cimento **34**, 495 (1965); Phys. Letters **10**, 226 (1964); **10**, 229 (1964); **10**, 240 (1964); **10**, 248 (1964); **11**, 167 (1964); Phys. Rev. **138**, B897 (1965), and Nuovo Cimento **35**, 659 (1965). M. Abolins, R. L. Lander, W. A. W. Mehlhop, N. H. Xuong, and P. M. Yeager, Phys. Rev. Letters **11**, 381 (1963). M. Abolins, D. D. Carmony, D-N. Hoa, R. L. Lander, C. Rindfleisch, and N. H. Xuong, Phys. Rev. **136**, B195 (1964). S. S. Yamamoto, J. R. Smith, D. C. Rahm, and J. L. Lloyd, *ibid.* **140**, B730 (1965).
[5] R. J. Plano and D. H. Tycko, Nucl. Instr. Methods **20**, 458 (1963).
[6] J. P. Berge, F. T. Solmitz, and H. D. Taft, Rev. Sci. Instr. **32**, 538 (1961).

TABLE I. Corrected path lengths.

P	2.35 BeV/c	2.62 BeV/c	2.90 BeV/c
Center-of-mass energy (E^*)	2.30 BeV	2.41 BeV	2.52 BeV
2-prong	$(5.55\pm0.16)\times10^6$ cm		$(5.46\pm0.16)\times10^6$ cm
4-prong	$(5.65\pm0.17)\times10^6$ cm	$(1.85\pm0.06)\times10^6$ cm	$(5.98\pm0.19)\times10^6$ cm

II. CROSS SECTIONS

The different beam momenta were determined by measurements on the curvature of beam tracks. Only tracks which interacted in the chamber and had more than 30 cm of track length before interacting were used for these measurements. The momenta of each of these tracks were computed using the known magnetic field in the chamber. For each of the different beam momenta enough tracks were measured so that the precision of the central value of the measured momentum distribution was greater than the uncertainty in the momentum due to the momentum resolution of the beam. The momentum spread in the beam was fixed by the beam geometry and was ±15 MeV/c.

The incident flux was measured by counting, in each roll, the number of beam tracks entering the fiducial volume. These were counted in every fiftieth frame. The flux was computed for each roll and these were added to give the flux at each of the momenta studied.

Before the cross sections were computed the flux was corrected to compensate for the following factors: muon contamination in the beam, scanning efficiency and criteria, losses in data handling and nonbeam pions.

The muon contamination is due to the decay of the pions in the beam. The design of the beam is such that the muons reaching the chamber with the same direction as the beam pions are due to pion decays between the last slit and the chamber. We estimate that the muon contamination is $(5\pm2)\%$ at each of the momenta.

The scanning efficiency was measured by a partial rescan of the film. A reduction of $(2\pm1)\%$ was made in the flux for missed four-pronged events while the correction for missed two-pronged events was $(12\pm2)\%$. To ensure that all momentum measurements were meaningful the events were required to have no track that scattered within 15 cm of the interaction vertex. This criteria necessitated a $(9.5\pm1)\%$ correction in the flux for the four-pronged events. The correction to the flux for two-pronged events was $(4.5\pm1)\%$.

Data-processing errors due to damaged cards, double punches in the cards, tape redundancies, and other such difficulties, necessitate a correction to the flux of $(10\pm1)\%$ for all types of events.

There are pions entering the chamber which are not part of the beam. These cannot always be recognized by the scanners. The direction of all interacting pions was
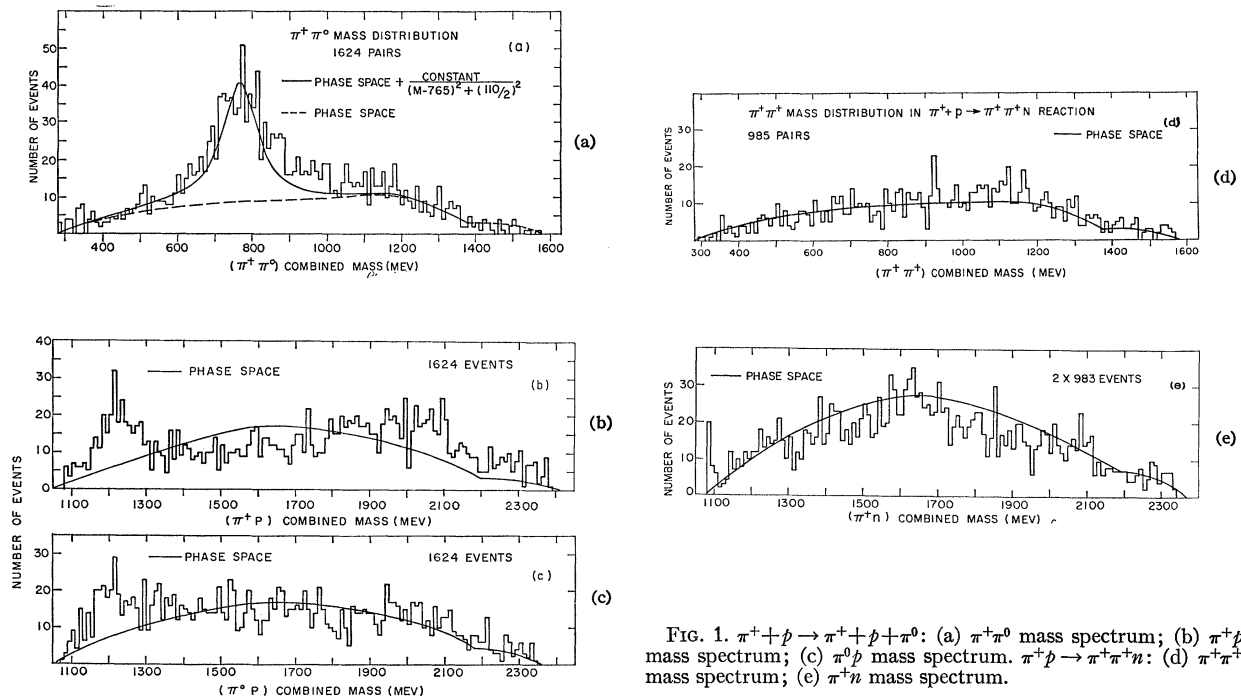

FIG. 1. $\pi^+ + p \rightarrow \pi^+ + p + \pi^0$: (a) $\pi^+\pi^0$ mass spectrum; (b) $\pi^+ p$ mass spectrum; (c) $\pi^0 p$ mass spectrum. $\pi^+ p \rightarrow \pi^+\pi^+ n$: (d) $\pi^+\pi^+$ mass spectrum; (e) $\pi^+ n$ mass spectrum.
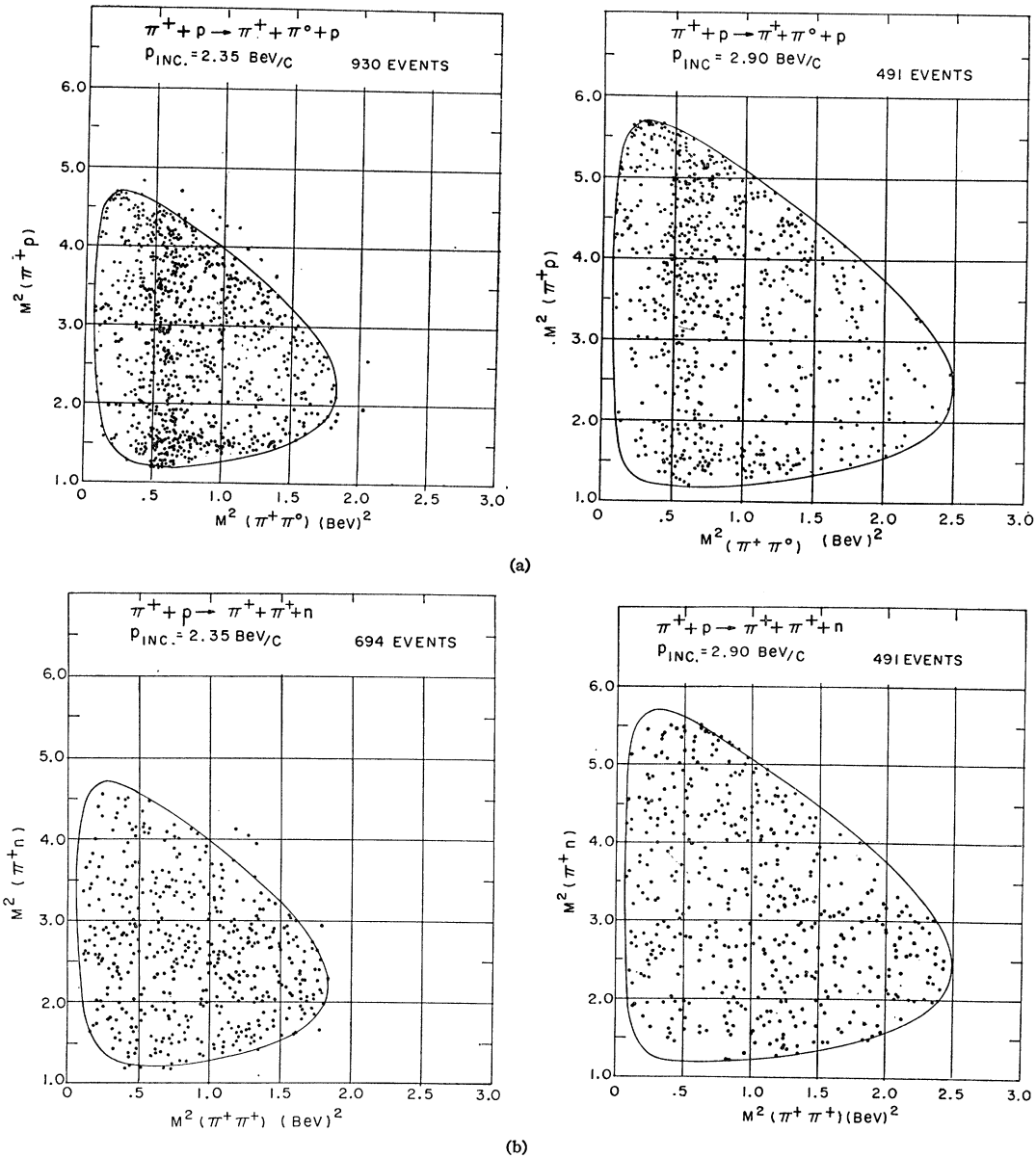
FIG. 2. Dalitz plot from the reaction (a) $\pi^+ + p \to \pi^+ + p + \pi^0$; (b) $\pi^+ + p \to \pi^+ + \pi^+ + n$.

checked in the analysis programs to see if the direction of the incident pion was in the direction of a beam pion. If not the event was rejected. Since these pions would

TABLE II. Corrected numbers of events.

P	2.35 BeV/c	2.62 BeV/c	2.90 BeV/c
E^*	2.30 BeV	2.41 BeV	2.52 BeV
$\pi^+ + p \to \pi^+ + p$	1500 ± 39		1300 ± 36
$\pi^+ + p \to \pi^+ + p + \pi^0$	970 ± 32		733 ± 27
$\pi^+ + p \to \pi^+ + \pi^+ + n$	491 ± 23		494 ± 23
$\pi^+ + p \to \pi^+ + p + \pi^+ + \pi^-$	726 ± 26	241 ± 16	660 ± 25
$\pi^+ + p \to \pi^+ + p + \pi^+ + \pi^- + \pi^0$	688 ± 26	267 ± 16	865 ± 29
$\pi^+ + p \to \pi^+ + \pi^+ + \pi^+ + \pi^- + n$	60 ± 8	27 ± 5	112 ± 10

have been included in any beam count, a correction of $(2 \pm 1)\%$ was made to the flux.

Table I gives the corrected flux together with an error which reflects the statistical accuracy of the beam count and the uncertainty in the various corrections.

When each of the events was measured an estimate was made by the measurer of the ionization of each of the tracks. The following code was used: 0—minimum ionization, 1—medium ionization, 2—heavily ionizing, 3—stopping proton, 4—stopping track, but not a proton. The beam track was used to define a minimum ionizing track for each event. A high degree of uniformity was achieved by the different measurers in the assignment of the ionization codes. The momentum of

TABLE III. Cross sections, in mb.

| P^* | 2.35 BeV/c | 2.62 BeV/c | 2.90 BeV/c |
E^*	2.30 BeV	2.41 BeV	2.52 BeV
Reaction			
$\pi^+ + p \to \pi^+ + p$	10.2 $\pm$0.5		8.3 $\pm$0.7
$\pi^+ + p \to \pi^+ + p + \pi^0$	4.7 $\pm$0.2		3.6 $\pm$0.2
$\pi^+ + p \to \pi^+ + \pi^+ + n$	2.38$\pm$0.14		2.42$\pm$0.14
$\pi^+ + p \to \pi^+ + p + \pi^+ + \pi^-$	3.44$\pm$0.16	3.49$\pm$0.25	2.95$\pm$0.14
$\pi^+ + p \to \pi^+ + p + \pi^+ + \pi^- + \pi^0$	3.26$\pm$0.16	3.86$\pm$0.25	3.87$\pm$0.17
$\pi^+ + p \to \pi^+ + \pi^+ + \pi^+ + \pi^- + n$	0.28$\pm$0.04	0.39$\pm$0.07	0.50$\pm$0.05

negative tracks was hitogrammed for the different ionization codes. These histograms provided a relationship between momentum and ionization code for pions. From the histograms for positive tracks and the pion ionization-momentum relations it was possible to extract the relation between ionization code and momentum for protons. The momentum-ionization code relations were determined for $|\lambda|$ ($\lambda=$dip angle)$\leq 40°$ and $40° < |\lambda| \leq 60°$. For dip angles greater than $\pm 60°$ the ionization-code information was not considered reliable enough to be used.

The ionization code was used in the following way. Each event was kinematically fitted to all possible hypotheses involving pions, kaons, and nucleons. A hypothesis consisted of assigning a mass to each of the tracks and assuming no or one missing π^0. The ionization was used here only to identify a stopping track so that the momentum from range could be used in the fit. If a particular fit had an acceptable X^2 (less than 20 for 4-constraint fits, and less than 6 for 1-constraint fits), the fitted momentum for each track was checked to see if it was between the momentum limits for the mass, ionization code, and dip angle of the particle. Only when all the tracks in a given hypothesis satisfied the ionization criteria was the hypothesis accepted.

If, for a given four-prong event, more than one hypothesis satisfied the minimum acceptance criteria (the number of these events is approximately 5% of the total number of four-pronged events), the probability based on X^2 for each of the acceptable criteria was calculated. If the probability for one hypothesis was three times as likely as any one of the others, then the event was considered unambiguous. If an event, after application of this criteria, was still ambiguous (less than 1% of the events) all the hypotheses acceptable on the basis of the minimum criteria were given equal weight in computing the cross sections.

Those events which had no hypothesis which satisfied the minimum criteria but at least one hypothesis which had a low enough X^2 were rescanned by a scanner. New independent ionization-code assignments were made. The ionization estimates after rescanning were compared with the output from GUTS and if the event now satisfied the ionization criteria it was accepted. This correction was negligible except for the reaction $\pi^+ + p \to \pi^+ + \pi^+ + \pi^+ + \pi^- + n$ where it amounted to ~10%.

The analysis of two-prong events with more than one acceptable hypothesis proceeded as follows. If the elastic-scattering hypothesis satisfied the minimum criteria ($X^2 \leq 20$ was required), then the event was accepted as an elastic scatter. To be accepted as either a $\pi^+ p \pi^0$ or $\pi^+ \pi^+ n$ event the X^2 was ≤ 6. The number of events that satisfied both the X^2 and the ionization criteria for both of these hypotheses was very small. These ambiguous events were not considered in the later analysis.
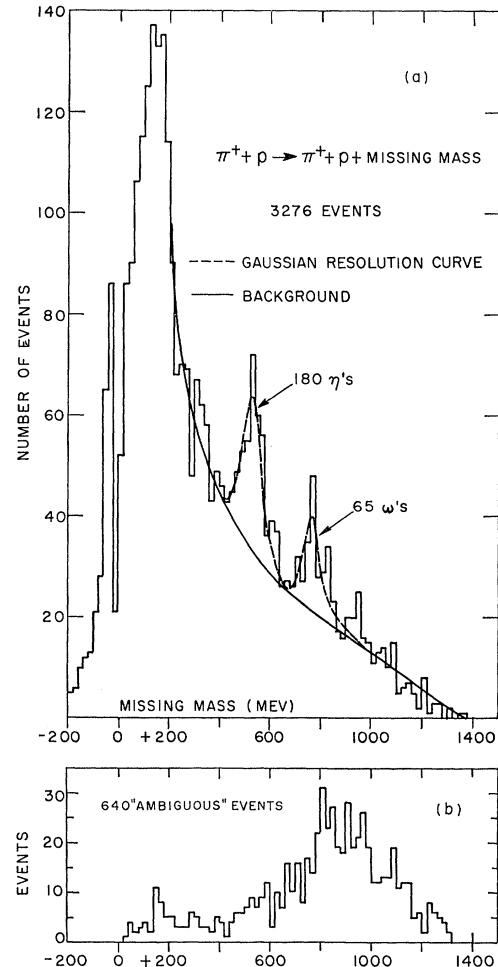

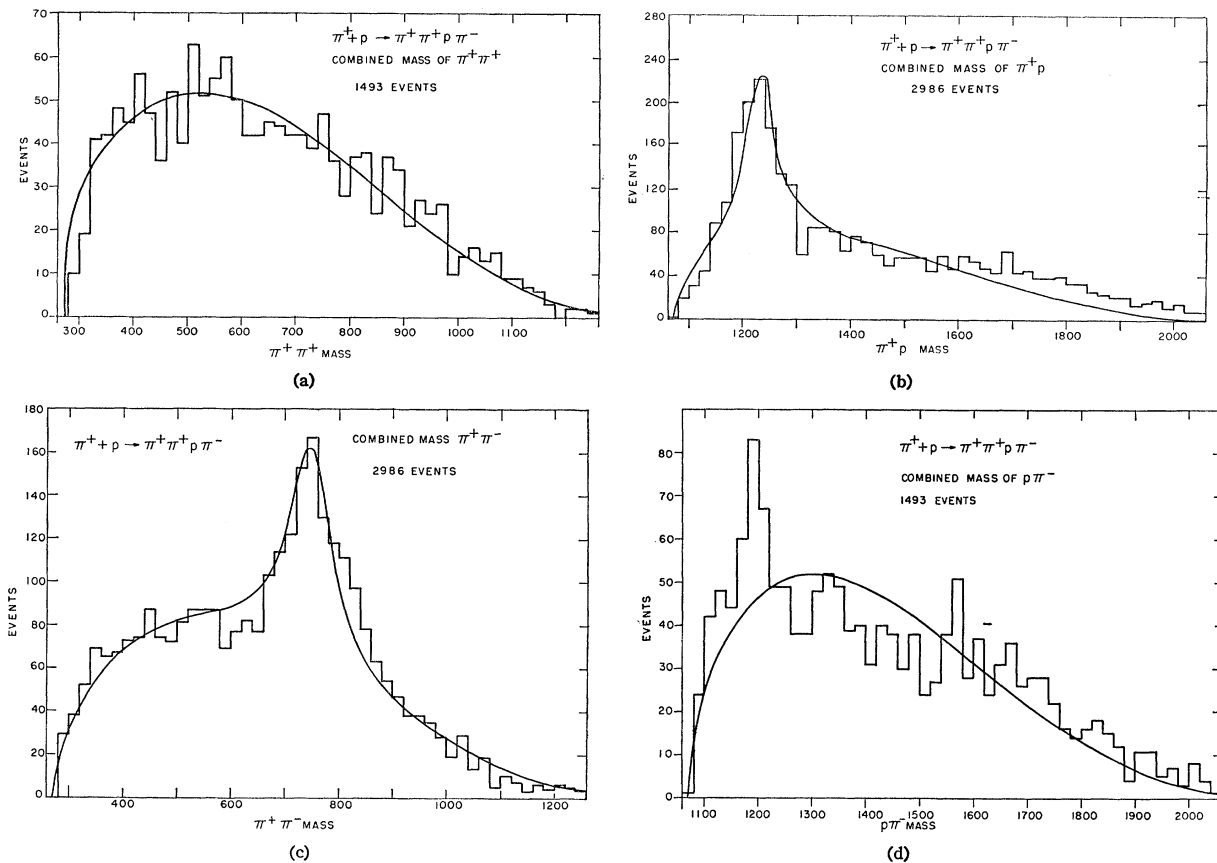FIG. 3. Missing-mass spectrum from the reaction $\pi^+ + p \to \pi^+ + p +$ "missing mass."

FIG. 4. $\pi^++p \to \pi^++p+\pi^++\pi^-$: (a) $\pi^+\pi^+$ mass spectrum; (b) π^+p mass spectrum; (c) $\pi^+\pi^-$ mass spectrum; (d) π^-p mass spectrum.

The corrected numbers of events are given in Table II while the cross sections (based on a density of hydrogen of 0.62 g/cm^3) are given in Table III. The errors on the cross sections are the result of adding in quadrature the uncertainty in the flux and the uncertainty in the number of events.

III. EFFECTIVE-MASS PLOTS

To search for resonances produced in the reactions $\pi^++p \to \pi^++p+\pi^0$ and $\pi^++p \to \pi^++\pi^++n$, events were selected that fit only one of these two hypotheses. The effective-mass spectra for the two-particle systems are plotted in Fig. 1. The Dalitz plots from these reactions are shown in Fig. 2. The missing-mass spectrum from the reaction $\pi^++p \to \pi^++p+$neutrals (Fig. 3) includes only those two-pronged events which did not fit either of the reactions $\pi^++p \to \pi^++p$ or $\pi^++p \to \pi^++\pi^++n$ and had a missing mass, assuming both prongs to be pions, of less than the neutron mass.

The two-body effective-mass spectrum from the reaction $\pi^++p \to \pi^++p+\pi^++\pi^-$ are shown in Fig. 4. The three-body effective-mass distributions are plotted in Fig. 5. Figures 6 and 7 show the two-body effective-mass spectra from the reaction $\pi^++p \to \pi^++p+\pi^+$

$+\pi^-+\pi^0$ and in Figs. 8 and 9 are plotted the three-body mass spectra from this reaction. Figure 10 shows the missing-mass (MM) spectra from the four-pronged events $\pi^++p \to \pi^++p+\pi^++\pi^-+$(MM). The two-particle mass spectra from the reaction $\pi^++p \to \pi^++\pi^++\pi^++\pi^-+n$ are plotted in Fig. 11. The three-body mass spectra from this reaction appear in Fig. 12. The spectra from the four-prong events include events with either only one acceptable hypothesis or we have one hypothesis ten times as probable as any other hypothesis.

The final states containing protons are characterized by production of both nucleonic and pionic resonances. The $(\tfrac{3}{2},\tfrac{3}{2})$ N^* is seen in the final states $\pi^++p+\pi^0$, $\pi^++p+\pi^++\pi^-$, and $\pi^++p+\pi^++\pi^-+\pi^0$ in the double-charged (π^+p) state.[7] The ρ^+ is produced only in reactions leading to the $\pi^++p+\pi^0$ final state.[8] The ρ^0 is seen only in the final state $\pi^++p+\pi^++\pi^-$. The ω^0 and η^0 are observed in the $\pi^++p+\pi^++\pi^-+\pi^0$ final state and also as bumps in the missing-mass spectrum

[7] M. Gell-Mann and K. M. Watson, Ann. Rev. Nucl. Sci. 4, 219 (1954).

[8] A. R. Erwin, R. March, W. D. Walker, and E. West, Phys. Rev. Letters 6, 628 (1961); D. Stonehill, C. Baltay, H. Courant, W. Fickinger, E. C. Fowler, H. Kraybill, J. Sandweiss, J. Sanford, and H. Taft, *ibid.* 6, 624 (1961).
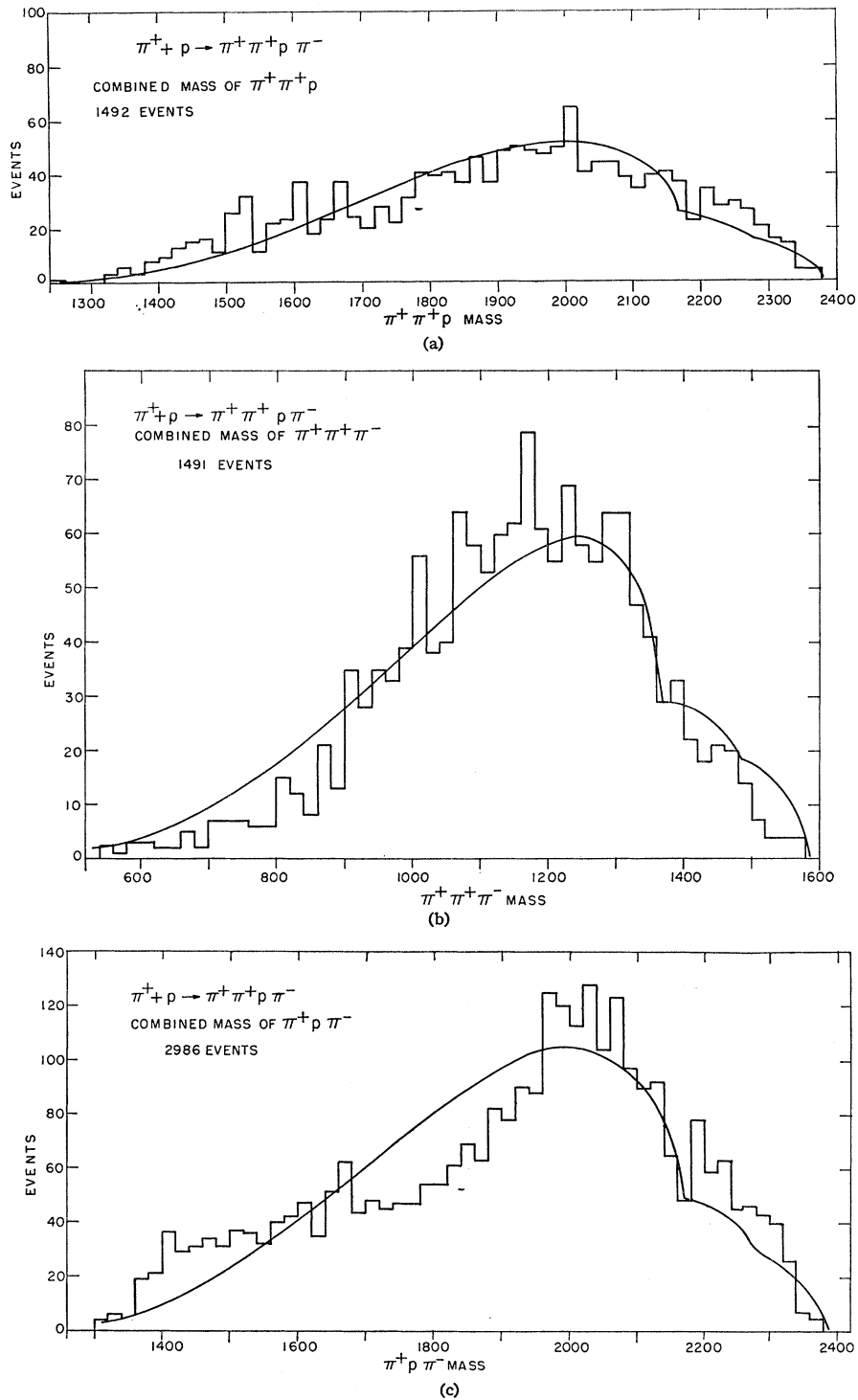
FIG. 5. $\pi^{+}+p \to \pi^{+}+p+\pi^{+}+\pi^{-}$: (a) $\pi^{+}\pi^{+}p$ mass spectrum; (b) $\pi^{+}\pi^{+}\pi^{-}$ mass spectrum; (c) $\pi^{+}p\pi^{-}$ mass spectrum.

$\pi^{+}+p \to \pi^{+}+p+$ (MM).[9,10] The measured rate for the neutral decay of the ω^{0} is,

$$R(\omega^{0} \to \text{neutral})/R(\omega^{0} \to \pi^{+}+\pi^{-}+\pi^{0})=0.099\pm0.004.$$

[9] B. C. Maglic, L. W. Alvarez, A. H. Rosenfeld, and M. L. Stevenson, Phys. Rev. Letters **7**, 178 (1961).
[10] A. Pevsner, R. Kraemer, M. Nussbaum, C. Richardson, P. Schlein, R. Strand, T. Toohig, M. Block, A. Engler, R. Gessaroli, and C. Meltzer, Phys. Rev. Letters **7**, 421 (1961).
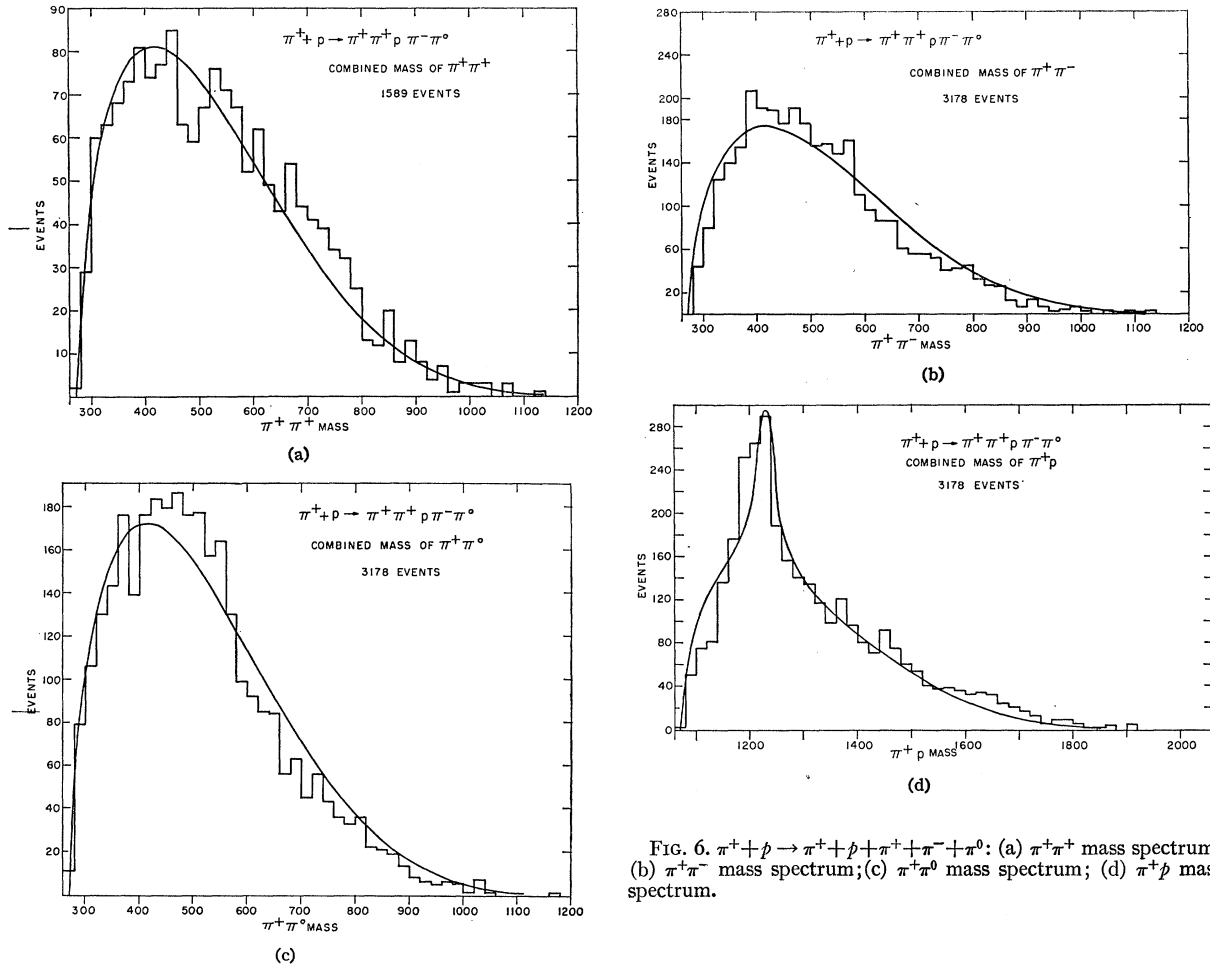
FIG. 6. $\pi^+ + p \rightarrow \pi^+ + p + \pi^+ + \pi^- + \pi^0$: (a) $\pi^+\pi^+$ mass spectrum; (b) $\pi^+\pi^-$ mass spectrum; (c) $\pi^+\pi^0$ mass spectrum; (d) π^+p mass spectrum.
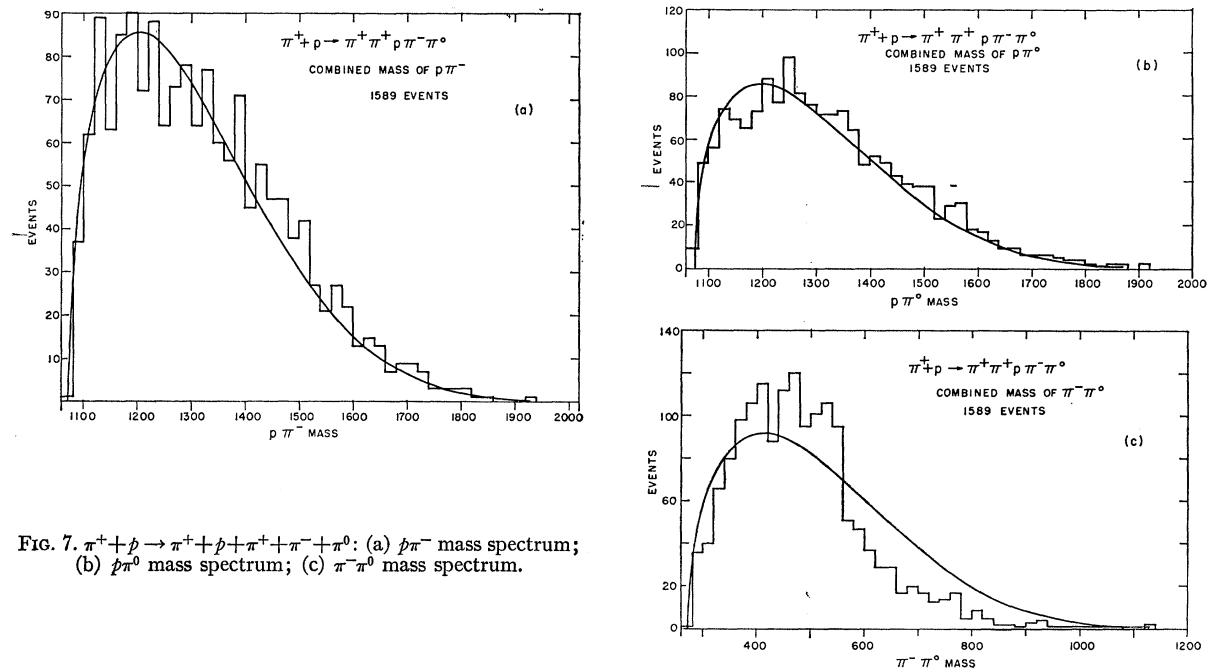
FIG. 7. $\pi^+ + p \rightarrow \pi^+ + p + \pi^+ + \pi^- + \pi^0$: (a) $p\pi^-$ mass spectrum; (b) $p\pi^0$ mass spectrum; (c) $\pi^-\pi^0$ mass spectrum.

TABLE IV. Cross sections, in mb.

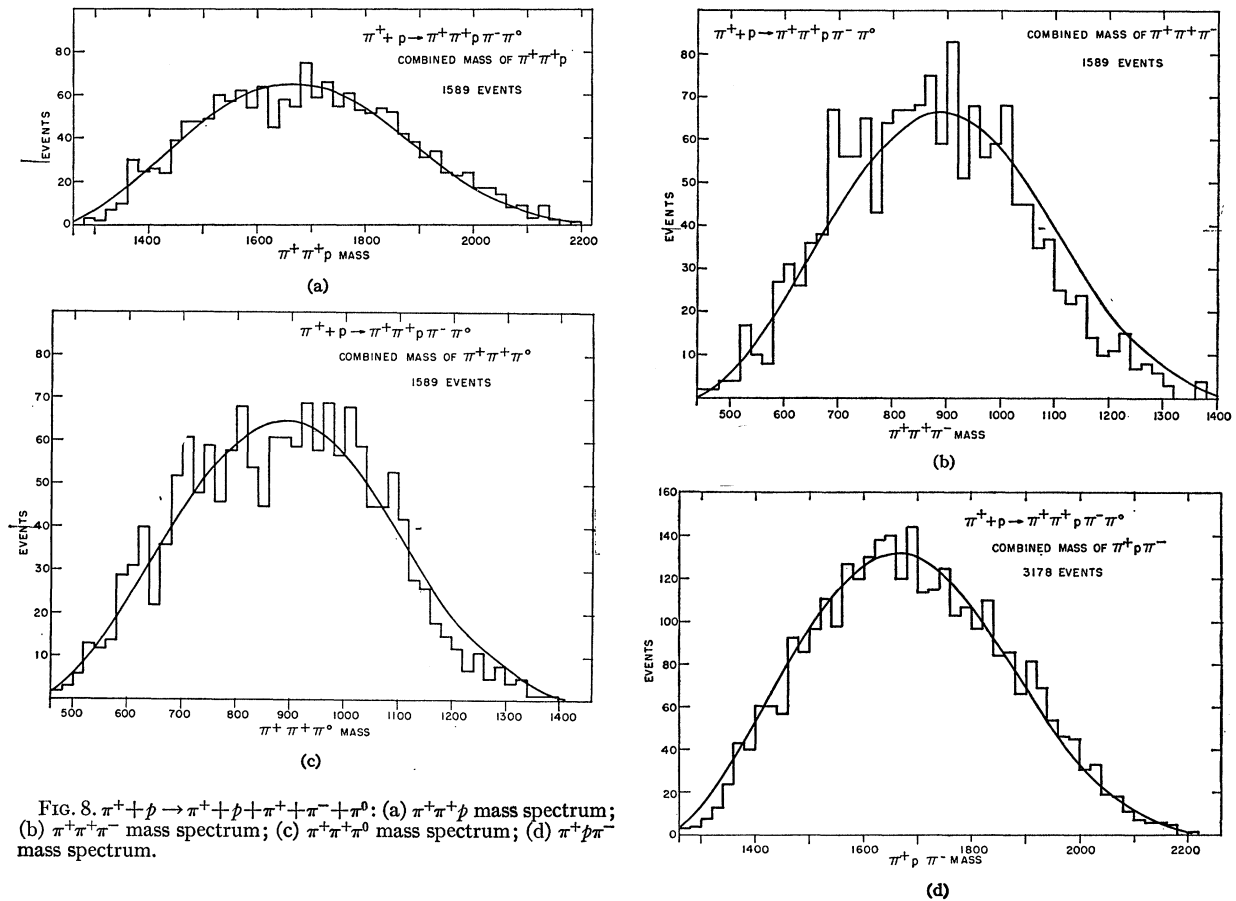| P Energy	2.35 BeV/c 2.30 BeV	2.62 BeV/c 2.41 BeV	2.90 BeV/c 2.52 BeV
Reactions			
$\pi^+ + p \rightarrow \pi^+ + p + \omega$ ⟍ neut	0.30±0.12		0.10±0.06
$\pi^+ + p \rightarrow \pi^+ + p + \omega^0$ ⟍ $\pi^+ + \pi^- + \pi^0$	2.10±0.19	2.61±0.31	1.97±0.17
$\pi^+ + p \rightarrow p + \rho^+$ ⟍ $\pi^+ + \pi^0$	1.5 ±0.3		1.1 ±0.2
$\pi^+ + p \rightarrow \pi^+ + p + \rho^0$ ⟍ $\pi^+ + \pi^-$	1.76±0.15	1.86±0.24	1.11±0.12
$\pi^+ + p \rightarrow \pi^+ + \pi^- + N^{*++}$ ⟍ $\pi^+ + p$	2.00±0.19	1.91±0.25	1.47±0.13
$\pi^+ + p \rightarrow \pi^+ + \pi^- + \pi^0 + N^{*++}$ ⟍ $\pi^+ + p$	1.41±0.13	1.52±0.23	0.96±0.10
$\pi^+ + p \rightarrow \pi^+ + p + \eta^0$ ⟍ $\pi^+ + \pi^- + \pi^0$	0.23±0.05	0.18±0.09	0.15±0.05
$\pi^+ + p \rightarrow \pi^+ + p + \eta^0$ ⟍ neut	0.55±0.15		0.55±0.15

FIG. 8. $\pi^+ + p \rightarrow \pi^+ + p + \pi^+ + \pi^- + \pi^0$: (a) $\pi^+ \pi^+ p$ mass spectrum; (b) $\pi^+ \pi^+ \pi^-$ mass spectrum; (c) $\pi^+ \pi^+ \pi^0$ mass spectrum; (d) $\pi^+ p \pi^-$ mass spectrum.
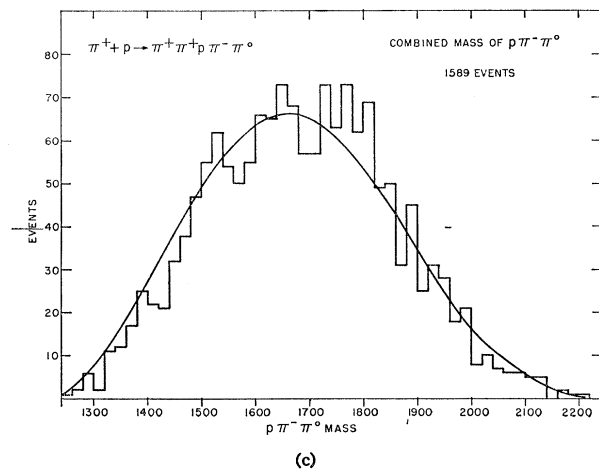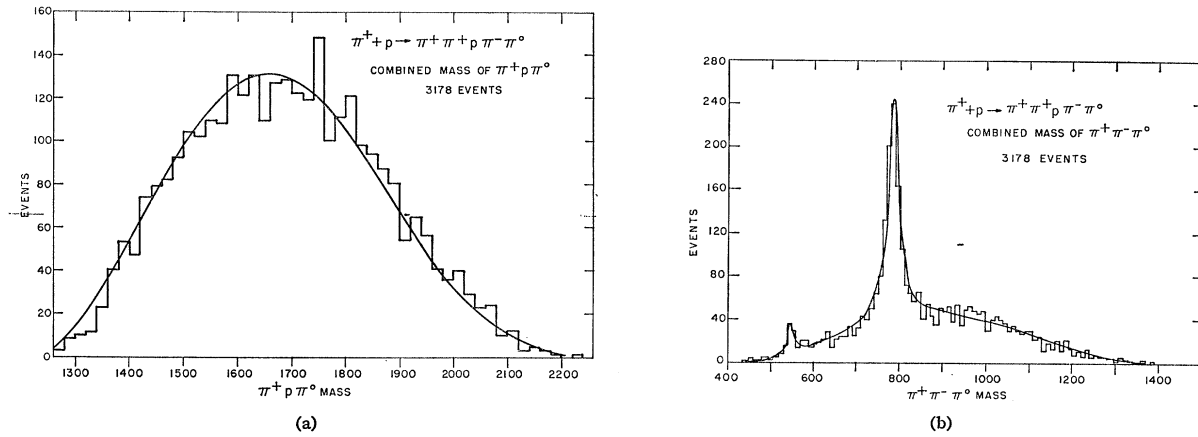
(a)

(b)

(c)

FIG. 9. $\pi^+ + p \to \pi^+ + p + \pi^+ + \pi^- + \pi^0$; (a) $\pi^+ p \pi^0$ mass spectrum; (b) $\pi^+ \pi^- \pi^0$ mass spectrum; (c) $p \pi^- \pi^0$ mass spectrum.
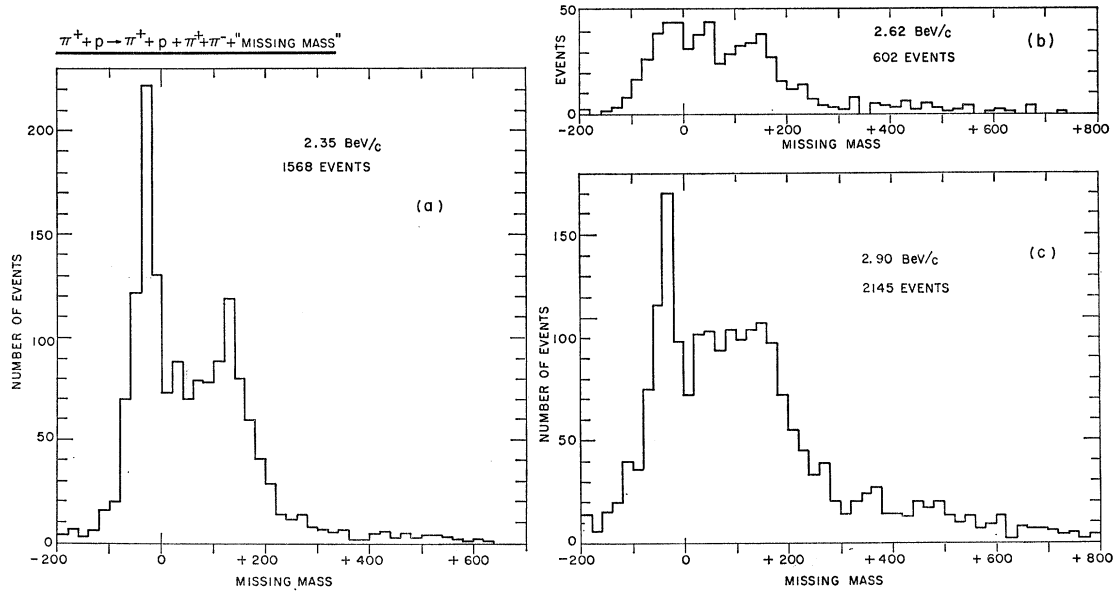

(a)

(b)

(c)

FIG. 10. Missing-mass spectrum from the reaction $\pi^+ + p \to \pi^+ + p + \pi^+ + \pi^- +$ "missing mass":
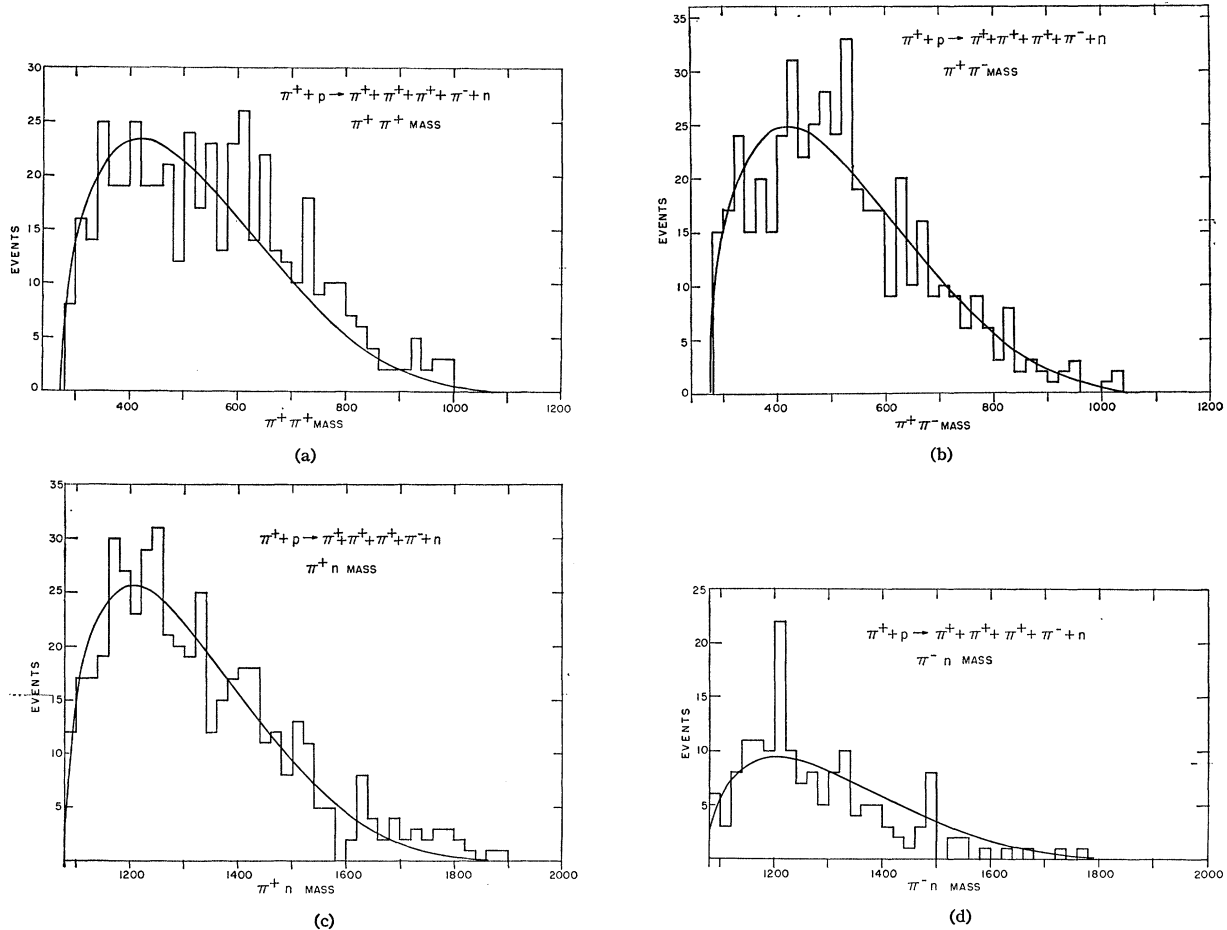(a) 2.35 BeV/c; (b) 2.62 BeV/c; (c) 2.90 BeV/c.

FIG. 11. $\pi^+ + p \rightarrow \pi^+ + \pi^+ + \pi^+ + \pi^- + n$: (a) $\pi^+\pi^+$ mass spectrum; (b) $\pi^+\pi^-$ mass spectrum; (c) π^+n mass spectrum; (d) π^-n mass spectrum.

The rate for the neutral η^0 decay is found to be:

$$R(\eta^0 \rightarrow \text{neutral})/R(\eta^0 \rightarrow \pi^+ + \pi^- + \pi^0) = 2.89 \pm 0.56.$$

The inclusion of ambiguous events, i.e., events in which the separation of the reaction $\pi^+ + p \rightarrow \pi^+ + p$ + (MM) from the reaction $\pi^+ + p \rightarrow \pi^+ + \pi^+ +$ (MM) could not be made on the basis of ionization, in the missing-mass plot (Fig. 3) does not change the number of events in either the η^0 or ω^0 peak. Inclusion of the ambiguous events increases the width of the ω^0 peak resulting in a larger error on the number of ω^0 decaying into neutrals. The error quoted is based only on the unambiguous events.

The observed cross sections for the production of the different resonances are collected in Table IV.

There is no evidence in the final state $\pi^+\pi^+n$ for any $T=2$ dipion resonance nor for the production of any resonance decaying into π^+n. The final state $\pi^+\pi^+\pi^+\pi^-n$ shows no evidence for the production of a resonance decaying into two or three particles. In particular the $n\pi^-$ mass spectrum shows no evidence for production of the $(\frac{3}{2},\frac{3}{2})$ isobar. The $\pi^+p\pi^+\pi^-$ final state shows produc-

tion of only the ρ^0 and N^{*++} resonances. Only the production of the η^0, ω^0, and N^{*++} resonances are seen in the $\pi^+\pi^+p\pi^-\pi^0$ final state.

There is no evidence in these data for the production of the X^0 resonance in $\pi^+ + p$ collisions.[11] The distribution of the missing mass for the four-prong events (Fig. 10) shows at most 5 ± 5 events in which the missing particle could be an η^0. If all of these events were to come from the decay of the X^0 resonance

$$\left(\text{i.e., } \pi^+ + p \rightarrow \pi^+ + p + \text{``}X^0\text{''} \underset{\pi^+ + \pi^- + \eta}{\searrow} \overset{\text{neut}}{\nearrow}\right),$$
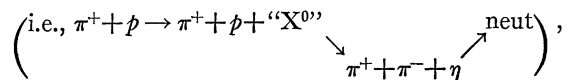
the cross section would be ~ 10 μb if it decayed only into $\pi^+\pi^-\eta$. The spectrum of the missing mass in the

[11] G. R. Kalbfleisch, L. W. Alvarez, A. Barbaro-Galtieri, O. I. Dahl, P. Eberhard, W. E. Humphrey, J. S. Lindsey, D. W. Merrill, J. J. Murray, A. Rittenberg, R. R. Ross, J. B. Shafer, F. T. Shively, D. M. Siegel, G. A. Smith, and R. D. Tripp, Phys. Rev. Letters 12, 527 (1964); M. Goldberg, M. Gundzik, S. Lichtman, J. Leitner, M. Primer, P. L. Connolly, E. L. Hart, K. W. Lai, G. London, N. P. Samios, and S. S. Yamamoto, ibid. 12, 546 (1964).
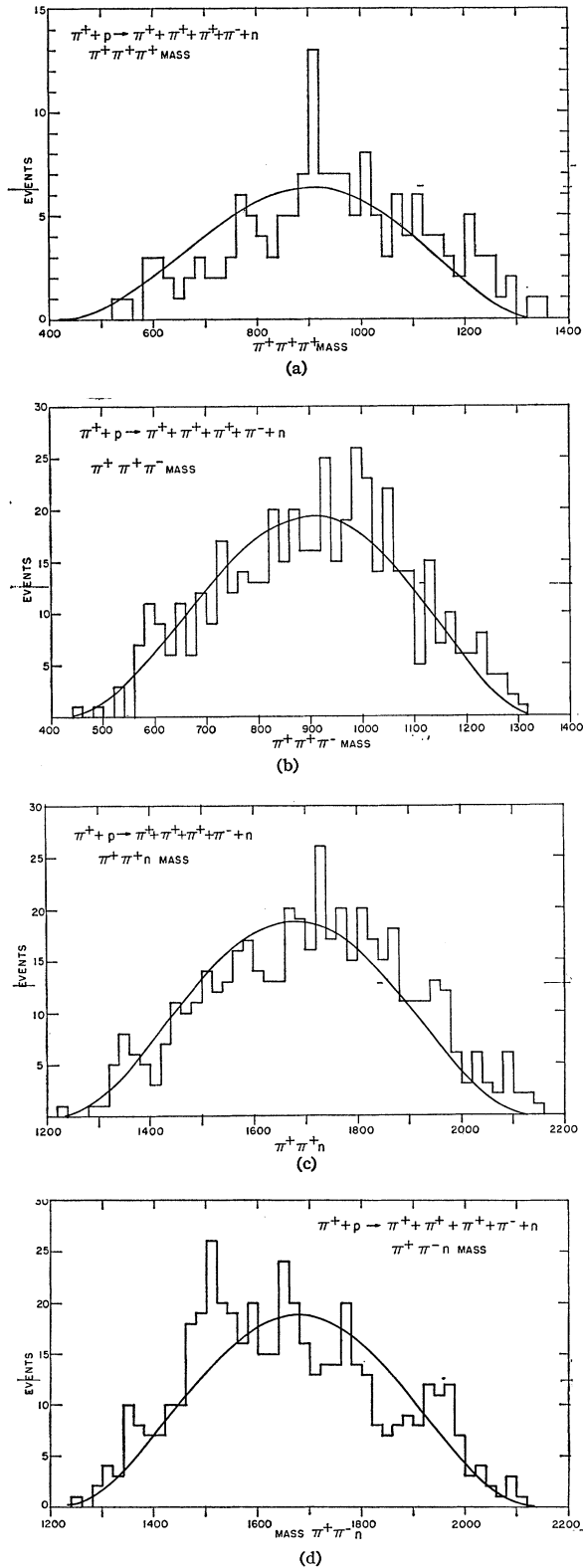
FIG. 12. $\pi^+ + p \rightarrow \pi^+ + \pi^+ + \pi^+ + \pi^- + n$: (a) $\pi^+\pi^+\pi^+$ mass spectrum; (b) $\pi^+\pi^+\pi^-$ mass spectrum; (c) $\pi^+\pi^+ n$ mass spectrum; (d) $\pi^+\pi^- n$ mass spectrum.
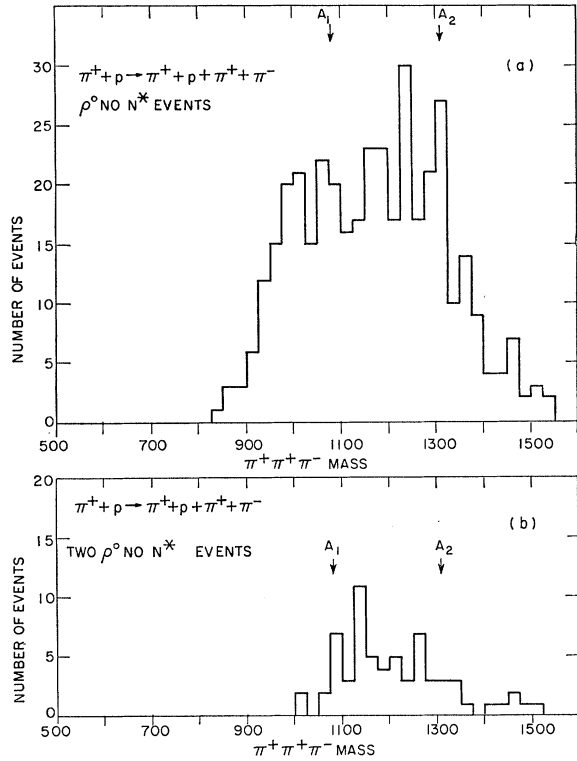

FIG. 13 (a) $\pi^+\rho^0$ mass spectrum from ρ^0 events produced without an N^{*++}. Only one $\pi^+\pi^-$ combination forms a ρ^0; (b) $\pi^+\rho^0$ mass spectrum from events in which both $\pi^+\pi^-$ combinations form a ρ^0 and no N^* is formed.

two-prong events has an upper limit of 20 ± 15 events which can be associated with the production and decay into neutrals of the X^0. This corresponds to a cross section of 60 ± 50 μb.

For the purpose of further analysis a ρ^0 will mean a $\pi^+\pi^-$ effective mass between 675 and 825 MeV, a ρ^+ will have a $\pi^+\pi^0$ effective mass in the interval 650 to 850 MeV, an N^*, a $\pi^+ p$ effective mass in the interval 1185 and 1285 MeV. An ω^0 will mean a $\pi^+\pi^-\pi^0$ mass between 755 and 815 MeV and an η^0 will have a $\pi^+\pi^-\pi^0$ effective mass between 530 and 570 MeV. For an event to be considered as an example of η^0 decay the mass of the other $\pi^+\pi^-\pi^0$ combination must not lie in the ω^0 mass interval. A histogram of the $\pi^+\rho^0$ mass from ρ^0 events produced without N^* and in which only one of the two $\pi^+\pi^-$ mass combinations lies in the ρ^0 interval is shown in Fig. 13(a). There is no evidence here for the production of either the A_1^+ or A_2^+ mesons.[12] The spectrum of $\pi^+\pi^+\pi^-$ masses for those events in which

[12] G. Goldhaber, J. L. Brown, S. Goldhaber, J. A. Kadyk, B. C. Shen, and G. H. Trilling, Phys. Rev. Letters **12**, 336 (1964); S. U. Chung, O. I. Dahl, L. M. Hardy, R. I. Hess, G. R. Kalbfleisch, J. Kirz, D. H. Miller, and G. A. Smith, *ibid.* **12**, 621 (1964).
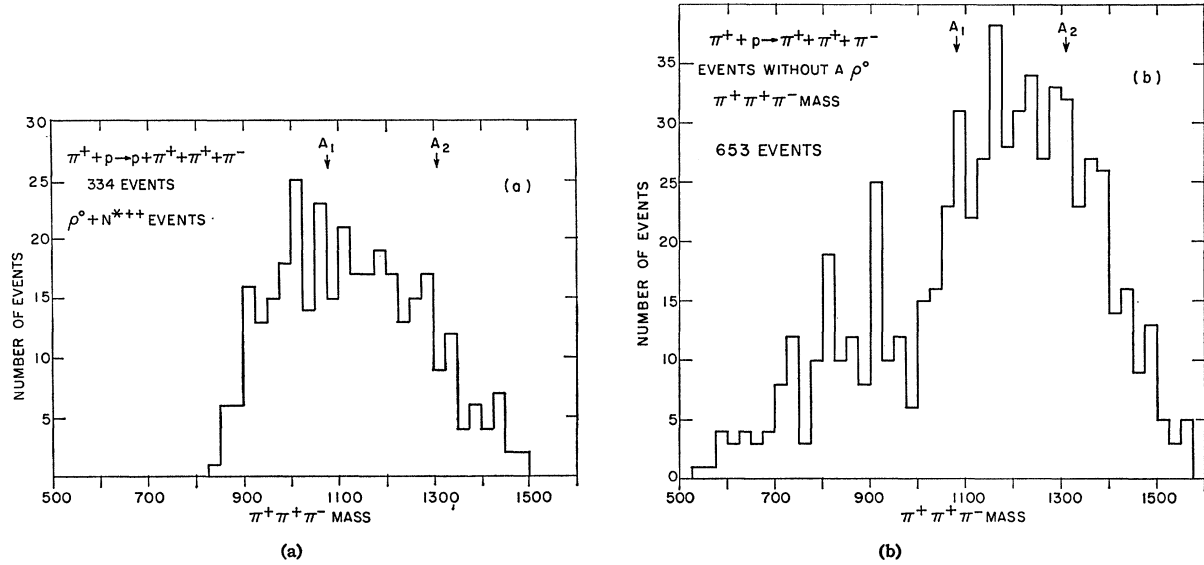
FIG. 14. (a) $\pi^+\rho^0$ mass spectrum from events in which $\pi^+\pi^-$ combination from a ρ^0 and an N^{*++} is formed;
(b) $\pi^+\pi^+\pi^-$ mass spectrum for $\pi^++p \rightarrow \pi^++p+\pi^++\pi^-$ events in which no ρ^0 is formed.

both $\pi^+\pi^-$ masses are in the ρ^0 region but no N^* is produced is almost totally within the mass range of the A mesons (950–1400 MeV) [Fig. 13(b)]. A Monte Carlo calculation of the $\pi^+\pi^+\pi^-$ mass spectrum, assuming isotropic ρ decay, has the same mass limits (~950–1400 MeV) indicating an enhancement due to the selection criteria in the regions of the A mesons. The $\pi^+\rho^0$ spectrum for ρ^0+N^* events in Fig. 14(a) and the $\pi^+\pi^+\pi^-$ mass spectrum for events without a ρ^0 is shown in Fig. 14(b).

The distribution of $\pi^+\omega$ masses in which the π^+p system recoiling against the ω^0 does not correspond to an N^{*++} is shown in Fig. 15. There is a small deviation from the phase space as already noted at higher energies.[13]

IV. ELASTIC SCATTERING

The differential cross sections from elastic-scattering events are shown in Fig. 16 for incident momenta of 2.35 and 2.90 BeV/c. The fitted curves are consistent with the exponential distributions

$$\frac{d\sigma}{d\Omega}=\frac{d\sigma}{d\Omega_0}e^{-At},$$

where

$$A=6.9\pm0.4(\text{BeV}/c)^{-2} \quad \text{at} \quad 2.35 \text{ BeV}/c$$

and

$$A=7.2\pm0.3(\text{BeV}/c)^{-2} \quad \text{at} \quad 2.90 \text{ BeV}/c.[14]$$

---

[13] M. Abolins, R. L. Lander, W. A. W. Mehlhop, N. H. Xuong, and P. M. Yager, Phys. Rev. Letters **11**, 381 (1963); G. Goldhaber, S. Goldhaber, J. A. Kadyk, and B. C. Shen, *ibid.* **15**, 118 (1965).

[14] A more complete analysis of π^+p elastic scattering will be published separately.

V. PRODUCTION OF THE ρ MESON

Production of the ρ^+ is seen only in the final state, $\pi^++p+\pi^0$, while the ρ^0 is observed only in the reaction $\pi^++p+\pi^++\pi^-$. The ρ^+ is observed at a mass of 765 ± 5 MeV. The ρ^0 is observed in the $\pi^++p+\pi^++\pi^-$ final state with a mass of 750 ± 5 MeV. The width of both these resonances is approximately 100 MeV.

Both the ρ^+ and ρ^0 are produced in very peripheral reactions, as can be seen both from the production angular distribution (Fig. 17) and the momentum-transfer distribution (Fig. 18). The Chew-Low plot (Fig. 19) for the ρ^0 shows that only in the mass region of the ρ^0 is there any striking clustering in the low Δ^2 region. A histogram of the π^+p mass recoiling against a
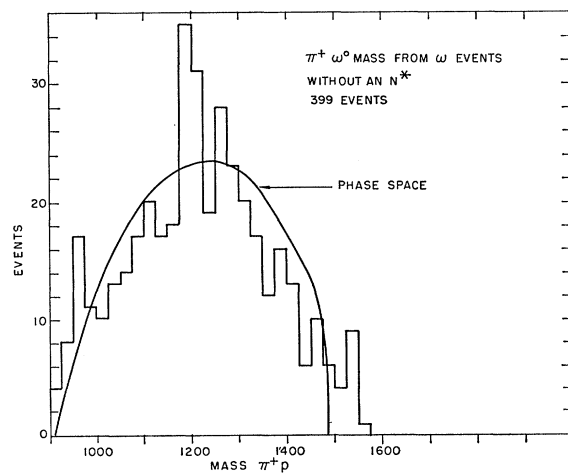

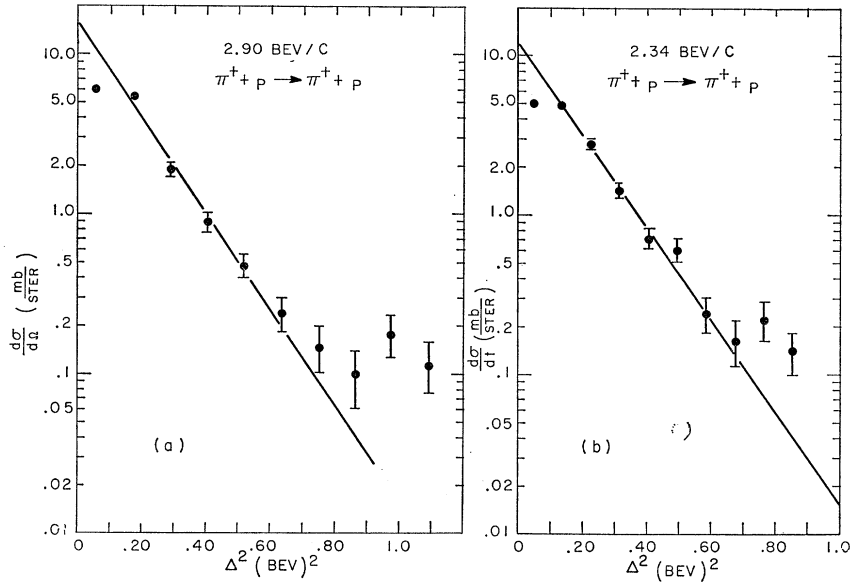FIG. 15. $\pi^+\omega^0$ mass spectrum for ω^0 events produced without an N^{*++}.
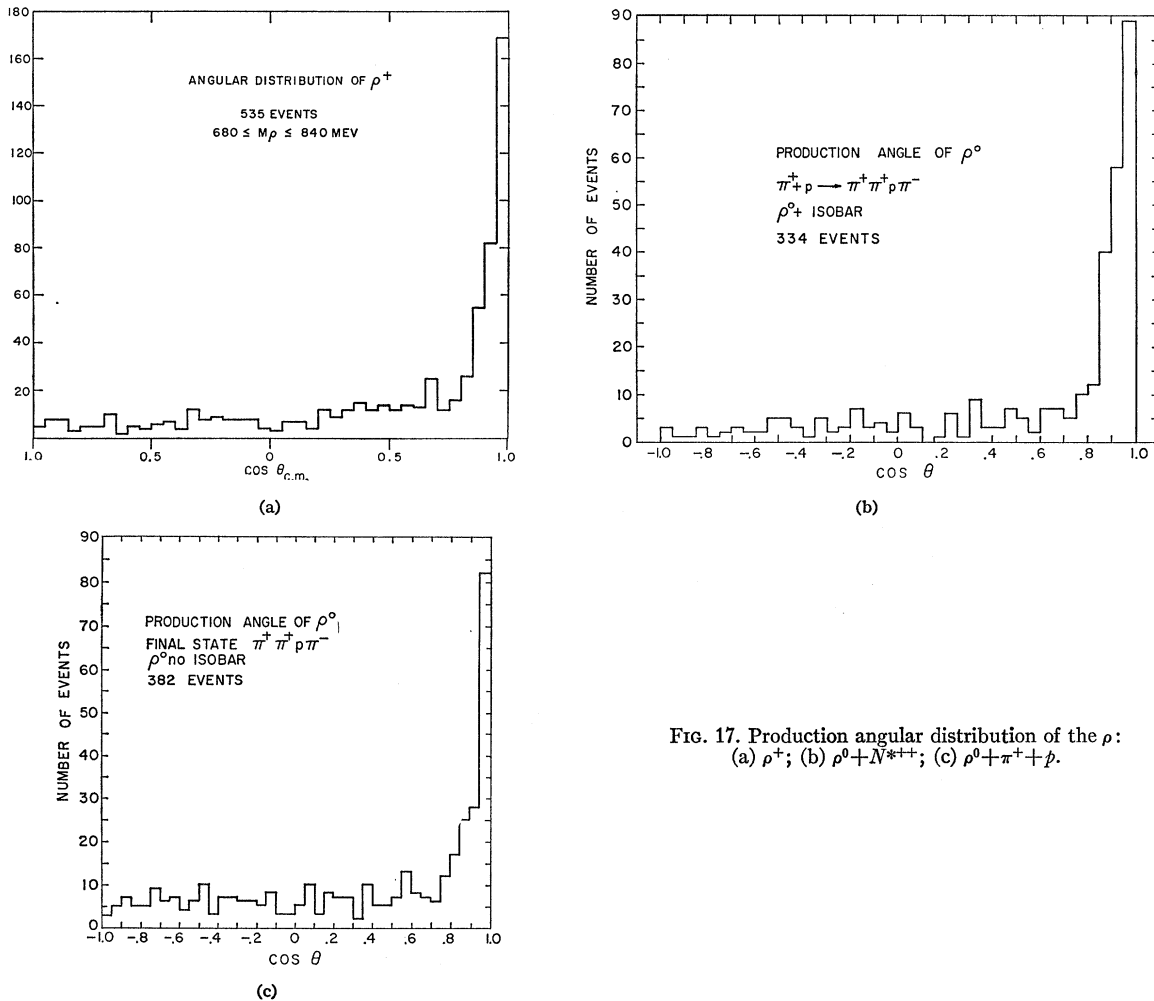
FIG. 16. Differential elastic scattering cross sections.

(a)

(b)

(c)

FIG. 17. Production angular distribution of the ρ:
(a) ρ^+; (b) $\rho^0 + N^{*++}$; (c) $\rho^0 + \pi^+ + p$.

Δ^2/M_π^2

$\pi^+ + p \rightarrow \rho^0 + N^{*++}$ (a)

MOMENTUM TRANSFER TO THE ρ^0

EVENTS

(a)

Δ^2/M_π^2

$\pi^+ + p \rightarrow \rho^0 + \pi^+ + p$ (b)

MOMENTUM TRANSFER TO ρ^0

ALL ENERGIES
380 EVENTS

EVENTS

(b)

Δ^2/M_π^2
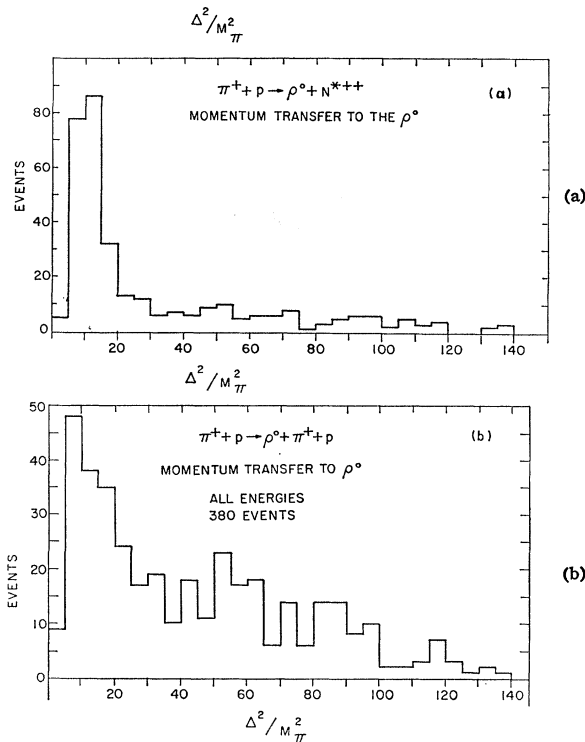
FIG. 18. Momentum transfer to the ρ:
(a) $\rho^0 + N^{*++}$; (b) $\rho^0 + \pi^+ + p$.

ρ^0 shows that an N^{*++} is often produced with the ρ^0 (Fig. 20). One-pion exchange[15] [Fig. 21(a)] provides the long-range force needed to explain the peripheralism in ρ production and provides a natural explanation for the simultaneous production of ρ^0 and N^{*++}. This force

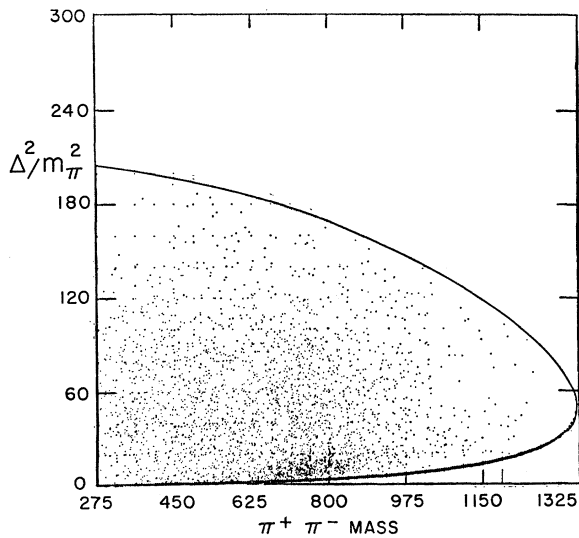Δ^2/m_π^2

$\pi^+ \pi^-$ MASS

FIG. 19. Chew-Low plot for $\pi^+ + p \rightarrow \pi^+ + p + \pi^+ + \pi^-$ events.

[15] C. J. Goebel, Phys. Rev. Letters **1**, 337 (1958); G. F. Chew, Phys. Rev. **113**, 1640 (1959); S. D. Drell, Phys. Rev. Letters **5**, 342 (1960); F. Salzman and G. Salzman, Phys. Rev. **120**, 599 (1960); E. Ferrari and F. Selleri, Nuovo Cimento **21**, 1028 (1961).
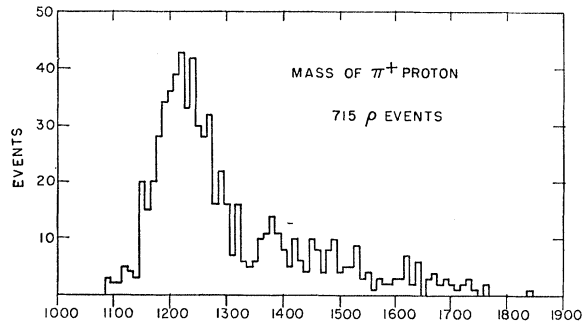

MASS OF π^+ PROTON

715 ρ EVENTS

EVENTS

FIG. 20. $\pi^+ p$ mass spectrum recoiling against ρ^0 meson.

is, however, incapable of reproducing the extreme peripheralism observed (Figs. 17 and 18). The one-pion-exchange model also predicts the decay correlations for the ρ. It is now customary to express these correlations in terms of the spin density matrix for a spin-one system.[16] We choose as the $\hat{k}$ axis the incident π^+ direction in the ρ rest system and as the $\hat{j}$ axis the ρ production plane normal. θ and ϕ are the polar and azimuthal angles of the π^+ in the ρ rest system. The most general distribution in θ and ϕ is given by

$$W(\theta,\phi) = \rho_{1,1} \sin^2\theta + \rho_{0,0} \cos^2\theta - \rho_{1,-1} \sin^2\theta$$
$$\times \cos^2\phi - \sqrt{2}\, \text{Re}\rho_{1,0} \sin 2\theta \cos\phi,$$

where

$$2\rho_{1,1} + \rho_{0,0} = 1$$

(ρ_{ij} is the spin-density matrix element). The one-pion-exchange model predicts that for the ρ only $\rho_{0,0}$ will be nonzero. Because the production mechanism for $\rho^0 + N^{*++}$ events could be different from the ρ^0 events produced without N^{*++}, we display the decay correlations separately. The experimental distribution in
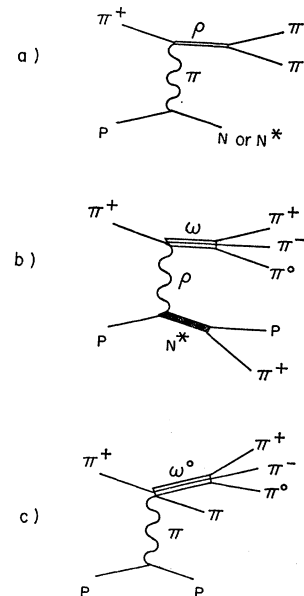

FIG. 21. (a) Unmodified one-pion-exchange diagram; (b) single-ρ exchange; (c) ω^0 production via one-pion exchange.

a)

b)

c)

[16] K. Gottfried and J. D. Jackson, Nuovo Cimento **22**, 309 (1964).

(a)

(b)

(c)
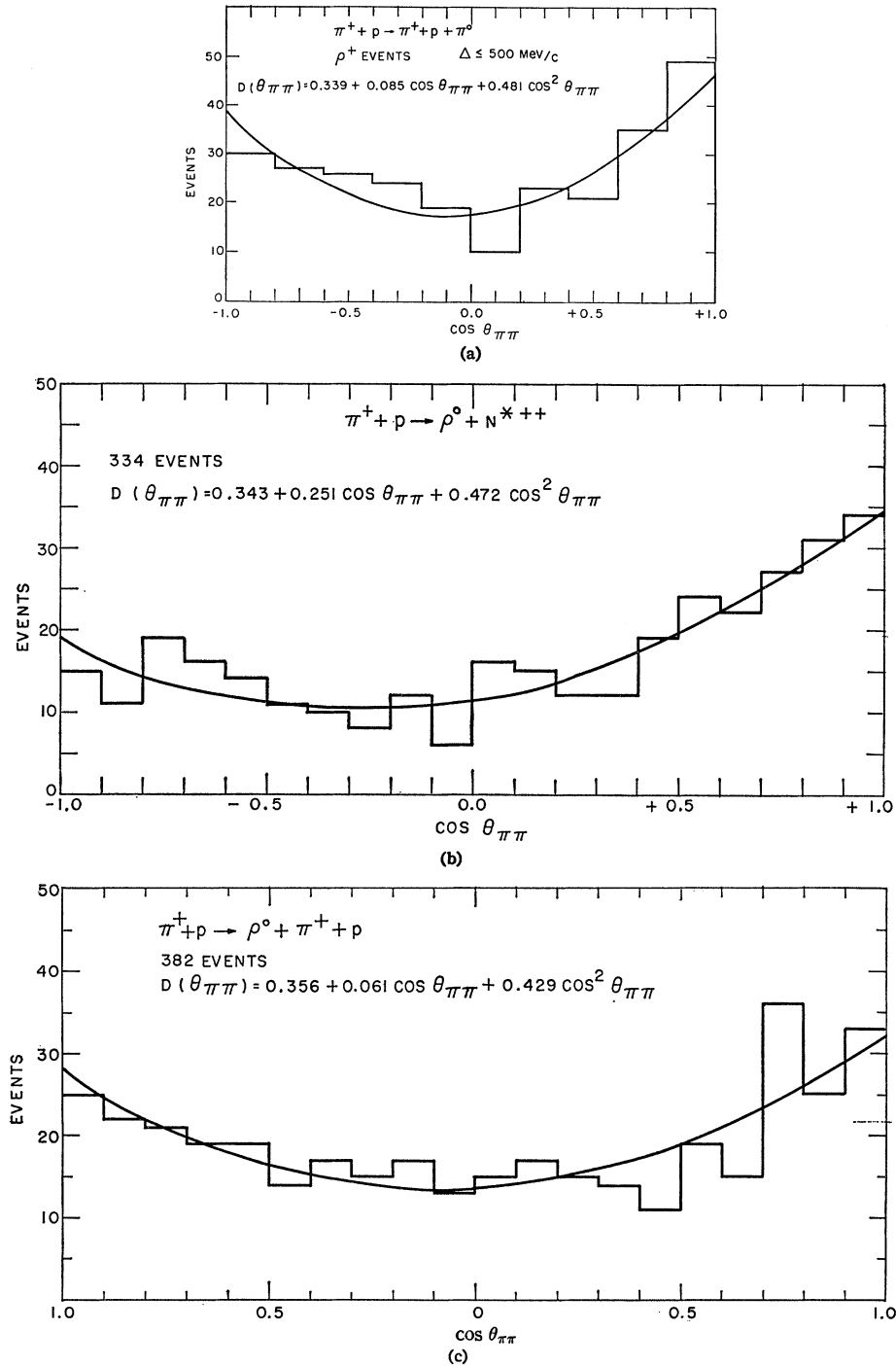
FIG. 22. ρ-decay correlations. θ is the angle in the ρ rest frame between the incoming π^+ and the π^+ from the ρ decay. (a) ρ^+; (b) ρ^0+N^{*++} events; (c) $\rho^0+\pi^++p$ events.

$\cos\theta$ is shown in Fig. 22 and for ϕ (the Treiman-Yang angle[17]) in Fig. 23. The distributions in ϕ are consistent with isotropy in agreement with the model. The distributions in $\cos\theta$ can be fitted with the expressions

ρ^++p :

$$D(\cos\theta) = (0.339\pm0.047)$$
$$+ (0.085\pm0.054)\cos\theta + (0.481\pm0.106)\cos^2\theta,$$

ρ^0+N^* :

$$D(\cos\theta) = (0.343\pm0.041)$$
$$+ (0.251\pm0.047)\cos\theta + (0.474\pm0.092)\cos^2\theta,$$

$\rho^0+\pi^++p$:

$$D(\cos\theta) = (0.356\pm0.038)$$
$$+ (0.061\pm0.044)\cos\theta + (0.429\pm0.086)\cos^2\theta.$$

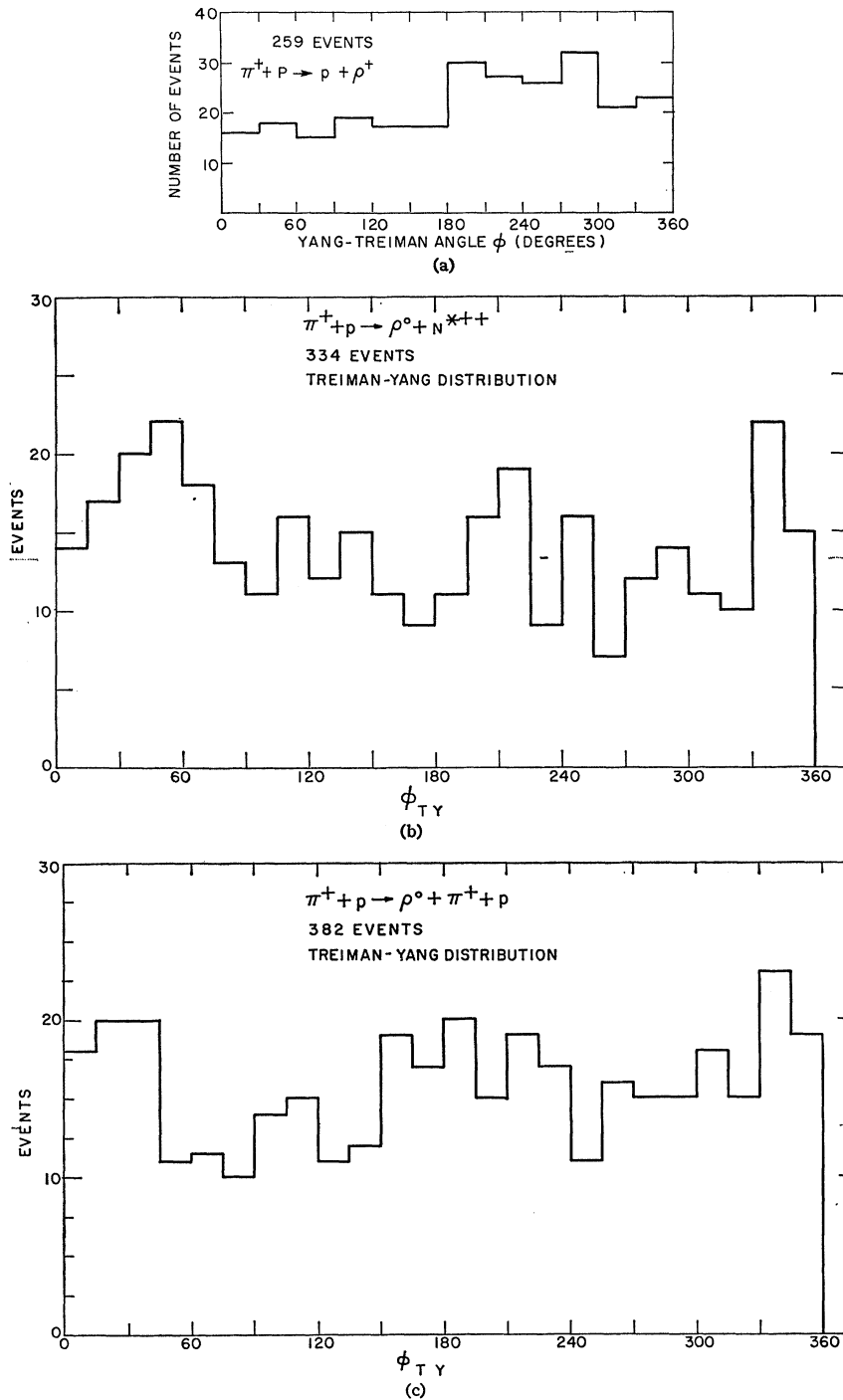[17] S. B. Treiman and C. N. Yang, Phys. Rev. Letters **8**, 140 (1962).

FIG. 23. Treiman-Yang distribution: (a) ρ^+; (b) ρ^0+N^{*++} events; (c) $\rho^0+\pi^++p$ events.

The one-pion-exchange diagram [Fig. 21a] does not provide a reasonable explanation of the experimental distributions. The values of $\rho_{0,0}$ corresponding to these distributions are

$$\rho^++p: \quad \rho_{0,0}=0.547\pm0.038,$$

$$\rho^0+N^{*++}: \quad \rho_{0,0}=0.543\pm0.033,$$

$$\rho^0+\pi^++p: \quad \rho_{0,0}=0.524\pm0.031,$$

significantly different from the expected value of 1.

We might hope to explain the disagreement of $\rho_{0,0}$ with the value expected for pure ρ production by considering interference with the background amplitude. In the $\pi^+\pi^-$ rest system the $\pi\pi$ angular distribu-
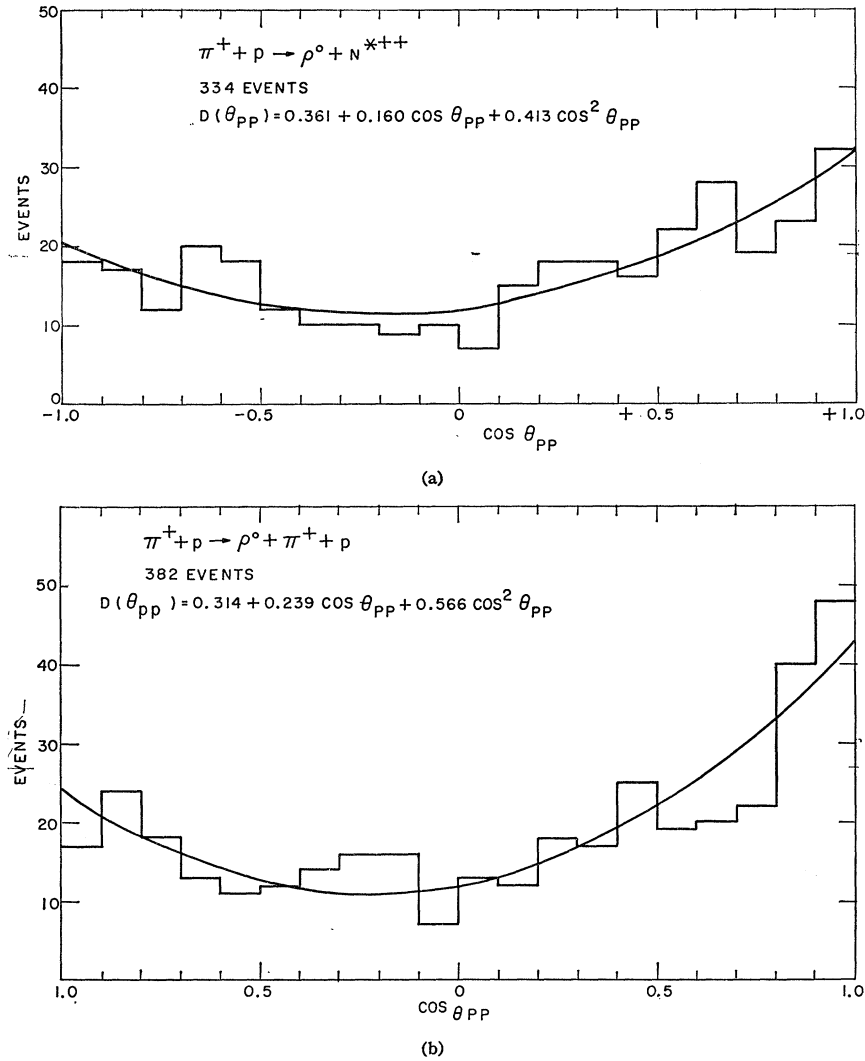
(a)

(b)

Fig. 24. Distribution in the angle between the incoming proton and the outgoing proton in the rest system of the proton and the π^+ not coming from the decay of the ρ^0. (a) $\rho^0 + N^{*++}$ events; (b) $\rho^0 + \pi^+ + p$ events.

tion is well fitted with terms only up to $\cos^2\theta$. Since the $\cos^2\theta$ term is presumably due to the P-wave amplitude associated with the ρ, the background amplitude must be S-wave. To account for the observed value of $\rho_{0,0}$ in this way, the background amplitude must be greater than the resonant ρ amplitude which is impossible.

Another failure of the model is shown in Fig. 24 where the distribution of the angle between the incident proton and the final proton in the π^+p rest system is displayed. The experimental distributions are fitted by the expressions

$\rho^0 + N^{*++}$: $D(\theta_N) = (0.361 \pm 0.047)$
$\quad + (0.160 \pm 0.047)\cos\theta_N + (0.413 \pm 0.092)\cos^2\theta_N$,

$\rho^0 + \pi^+ + p$: $D(\theta_N) = (0.314 \pm 0.038)$
$\quad + (0.239 \pm 0.044)\cos\theta_N + (0.566 \pm 0.086)\cos^2\theta_N$.

The model would predict $1 + 3 \cos^2\theta_N$ for $\rho^0 + N^{*++}$ events and makes no prediction for $\rho^0 + \pi^+ + p$ events.

An attempt has been made to correct these defects in the model by including the effects of absorption in the initial and final states.[18] The effect of the absorption is to deplete the low partial waves in the incoming plane waves. This increases the forward peaking in the differential cross section and decreases $\rho_{0,0}$. The measured values of $\rho_{0,0}$ are not inconsistent with the values expected from calculations done with the model at similar energies. The model also predicts that $\mathrm{Re}\rho_{1,0}$ will be ≈ -0.15, and this is in good agreement with our data which gives $\mathrm{Re}\rho_{1,0} = -0.10 \pm 0.01$ for $\rho^0 + N^*$ events. For $\rho^0 + \pi^+ + p$ events $\mathrm{Re}\rho_{1,0} = 0.052 \pm 0.01$. The major difficulty with the model is that it fails to explain the large asymmetry observed in the ρ^0 produced with the N^*. The effect here cannot be a result of symmetrization of the wave function under interchange of

[18] K. Gottfried and J. D. Jackson, Nuovo Cimento **24**, 735 (1964); M. H. Ross and G. L. Shaw, Phys. Rev. Letters **12**, 627 (1964); Loyal Durand, III, and Yam Tsi Chiu, Phys. Rev. **139**, B646 (1965).
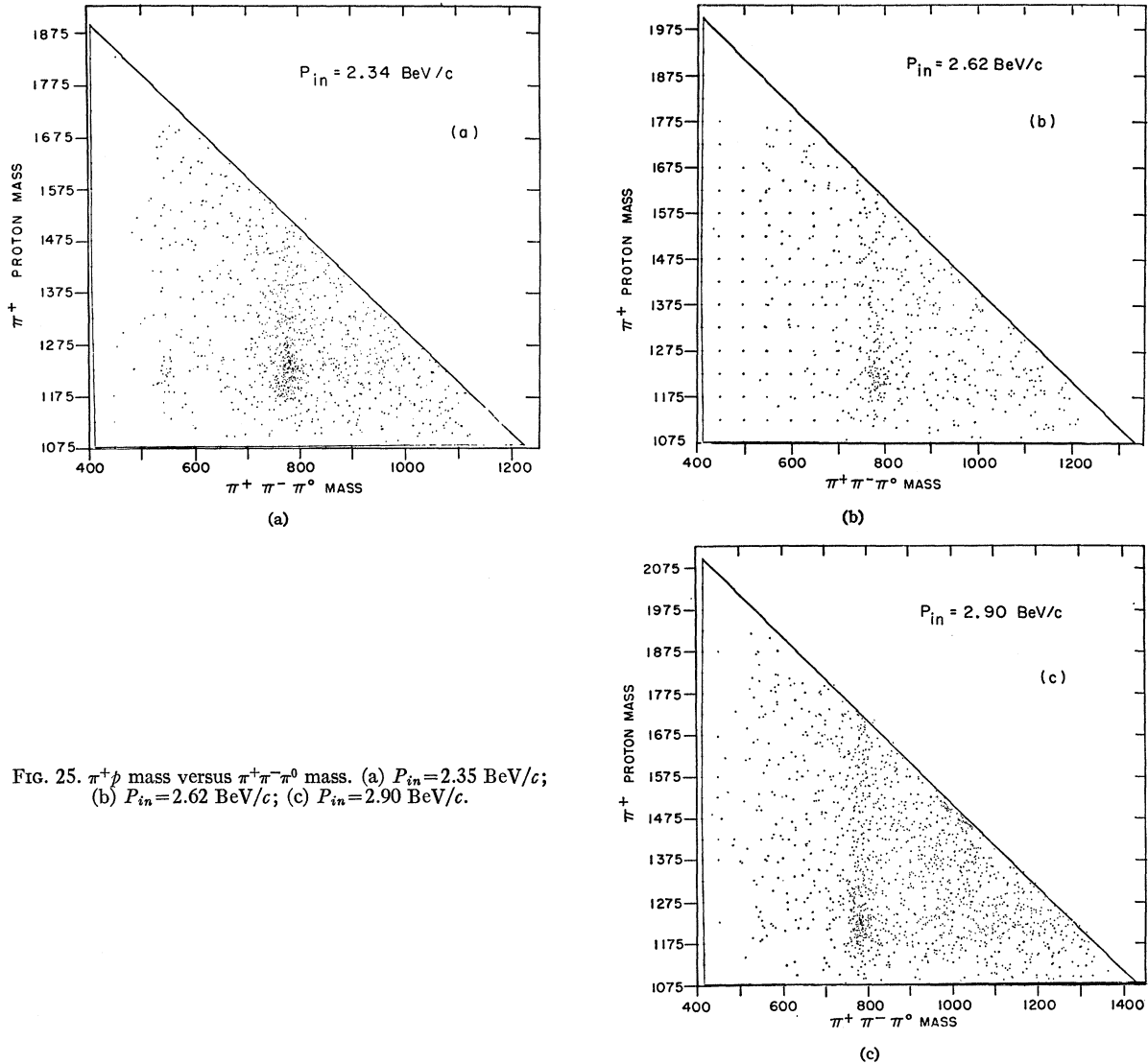
(a)

(b)

(c)

FIG. 25. $\pi^+ p$ mass versus $\pi^+\pi^-\pi^0$ mass. (a) $P_{in}=2.35$ BeV/c; (b) $P_{in}=2.62$ BeV/c; (c) $P_{in}=2.90$ BeV/c.

the two π^+, because these ρ^0 events are so selected that the interchange of the two π^+ will not result again in a ρ^0. Assuming that the background amplitude in the ρ region is also due to one-pion exchange, the existence of a strong $T=0$ S-wave $\pi\pi$ interaction, possibly a resonant $\pi\pi$ interaction, has been proposed to account for the asymmetry.[19] This model could not account for the large difference in the asymmetry between ρ^0 produced with and without N^{*++}, nor for the large asymmetry observed in the N^{*++} decay.

VI. ω^0 PRODUCTION

The most prominent features of the final state, $\pi^+ p\pi^+\pi^-\pi^0$, are the strong production of ω^0, η^0, and

N^{*++} resonances. A scatter plot (Fig. 25) of the $\pi^+ p$ mass and $\pi^+\pi^-\pi^0$ mass shows a heavy concentration in the region corresponding to simultaneous production of the ω^0 and N^{*++} resonances.

The production angular distribution of ω^0 produced with N^{*++} and without N^{*++} [Fig. 26(a)] and the momentum transfer distribution to the ω^0 [Fig. 27(a)] show that the ω^0 is produced via a peripheral reaction. For ω^0 produced with a N^{*++}, the longest range force generated by the exchange of a single particle corresponds to ρ^- exchange [Fig. 21(b)]. Since the ρ is much heavier than the pion, we would not expect ω^0 production to be as sharply peaked as ρ^0 production. This is indeed the case [Figs. 26(a) and 17(a)]. The ω^0 having spin one, the decay of the ω^0 can be analyzed in

[19] L. Durand, III, and Y. T. Chiu, Phys. Rev. Letters **14**, 329 (1965). These authors propose a $T=0$ S-wave pion-pion resonance with a mass and width approximately equal that of the ρ^0. Evidence for a two-pion resonance has been obtained by M. Feldman

et al., Phys. Rev. Letters **14**, 1077 (1965) at a mass of 720 MeV and a width $\Gamma\sim 50$ MeV. The relevance of these observations to the observed asymmetry is not obvious.
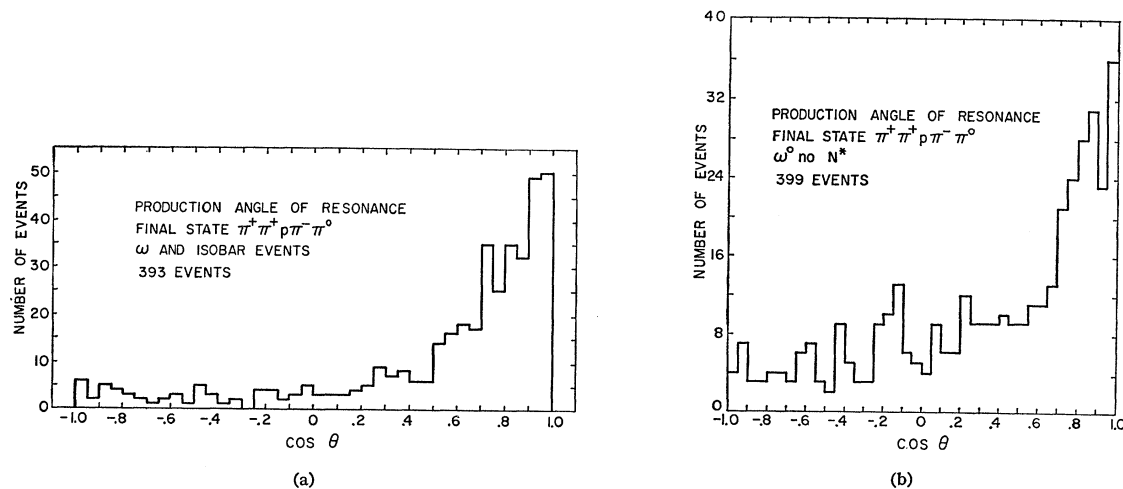
FIG. 26. Production angular distribution for the ω^0: (a) $\omega^0 + N^{*++}$ events; (b) $\omega^0 + \pi^+ + p$ events.

terms of the density matrix used to study the ρ. Using a simple model of ρ exchange, we would expect that $\rho_{0,0}$ and $\mathrm{Re}\rho_{1,0}$ would be zero. The experimental distribution shown in Fig. 28 can be fitted with the expression

$$D(\theta) = (0.369 \pm 0.036) + (0.038 \pm 0.050)$$
$$\times \cos\theta + (0.394 \pm 0.095)\cos^2\theta$$

(θ is the angle in the ω^0 rest system between the direction of the incident π^+ and the normal to the ω^0 decay plane). This corresponds to

$$\rho_{0,0} = 0.508 \pm 0.034$$

in drastic disagreement with the simple ρ-exchange
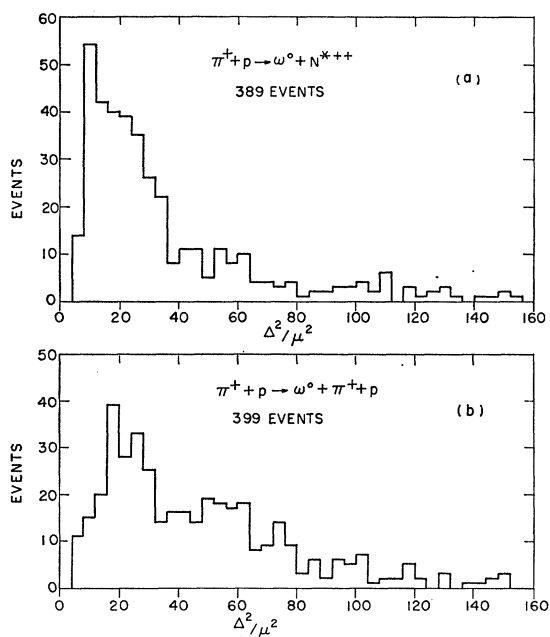
FIG. 27. Momentum transfer to the ω^0:
(a) $\omega^0 + N^{*++}$ events; (b) $\omega^0 + \pi^+ + p$ events.

model. The model has been modified recently with the inclusion of absorptive effects and form factors. Calculations by Svensson give $\rho_{0,0} \approx 0.6$ and are in reasonable agreement with the experimental angular distributions and decay correlations that are obtained.[20]

The angular distribution of ω^0 produced without N^{*++} is shown in Fig. 26(b) and the momentum-transfer distribution in Fig. 27(b). The ω^0 produced without N^{*++} can be produced via one-pion exchange [Fig. 21(c)]. The distribution of the Treiman-Yang angle [Fig. 29] is consistent with this hypothesis. If the diagram in Fig. 21(c) dominates the reaction, we would expect the proton to be sharply peaked in the backward direction with much the same width as the forward peak in ρ^+ production. The observed distribution (Fig. 30) is much broader than the ρ^+ distribution. A test of the one-pion-exchange model [Fig. 21(c)] involves looking at the decay correlation of the ω^0, choosing as the $\hat{k}$ axis the incident π^+ direction in the $\pi^+ + \omega^0$ rest system, and as the $\hat{j}$ axis the normal to the plane of the π-π scattering in this rest system. With this choice of axis, $\rho_{0,0}$ should be zero. The experimental distribution projected onto the $\hat{j}$ and $\hat{k}$ axis (Fig. 31) can be fitted with the expressions

$$D(\theta_{k,\omega}) = (0.317 \pm 0.038) + (0.060 \pm 0.044)\cos\theta$$
$$+ (0.549 \pm 0.086)\cos^2\theta,$$
$$D(\theta_{j,\omega}) = (0.598 \pm 0.038) + (0.036 \pm 0.044)\cos\theta$$
$$+ (-0.249 \pm 0.086)\cos^2\theta.$$

This corresponds to a value of $\rho_{0,0} = 0.577 \pm 0.031$ in violent disagreement with the predictions of the one-pion-exchange diagram. This failure is due either to absorptive effects, or more likely that one-pion exchange does not represent the mechanism responsible for the reaction.

[20] J. D. Jackson, J. T. Donohue, K. Gottfried, R. Keyser, and B. E. Y. Svensson, Phys. Rev. **139**, B428 (1965); H. Pilkuhn and B. E. Y. Svensson, Nuovo Cimento **38**, 518 (1965).
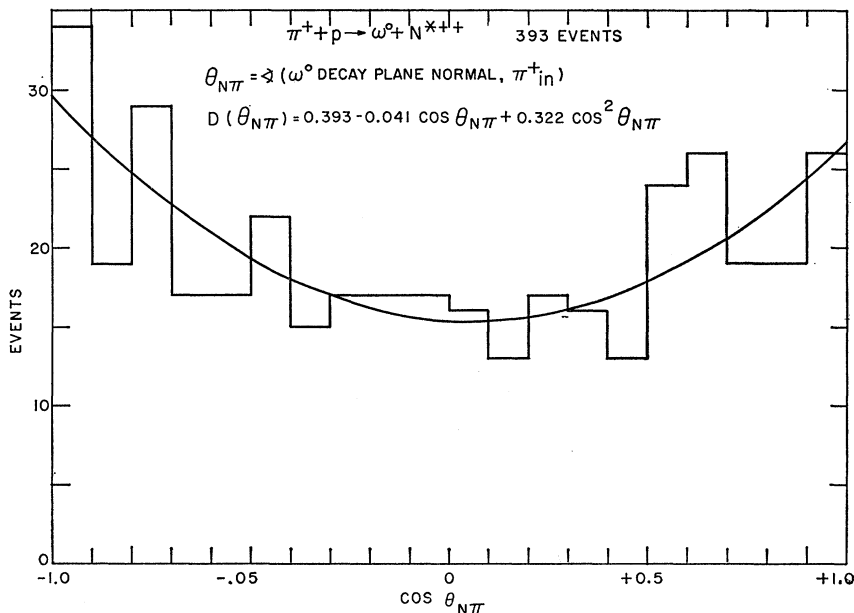
FIG. 28. Distribution of the angle between the ω^0-decay plane normal and the incident-π^+ direction in the ω^0 rest system.

VII. DECAY OF THE ω^0

The decay of the ω^0 in its rest system is studied with the aid of a Dalitz plot.[21] The data for events in the ω^0 mass region $755 < M(\pi^+\pi^-\pi^0) \leq 815$ MeV are shown in Fig. 32. The data from two control regions $700 \leq M(\pi^+\pi^-\pi^0) \leq 740$ MeV and $830 \leq M(\pi^+\pi^-\pi^0) \leq 870$ MeV are shown in Fig. 33. Only the Dalitz plot for the ω^0 events show the depletion at the boundary of the plot characteristic of a 1^- particle. The dependence of the ω^0 decay matrix element on the momenta of the pions is

just the three-pion wave function. The simplest possible 1^- wave function for three pions is

$$\psi = (\mathbf{k}_+ - \mathbf{k}_-) \times (\mathbf{k}_+ + \mathbf{k}_-),$$

where $\mathbf{k}_+$ and $\mathbf{k}_-$ are the π^+ and π^- momenta in the ω^0 rest frame. This matrix element gives a good fit to the experimental distribution (Fig. 34).

The existence of a two-pion decay mode for the K_2^0 has led to the suggestion that C (charge conjugation) might be violated in the electromagnetic interactions of the strongly interacting particles.[22] A C-violating ampli-
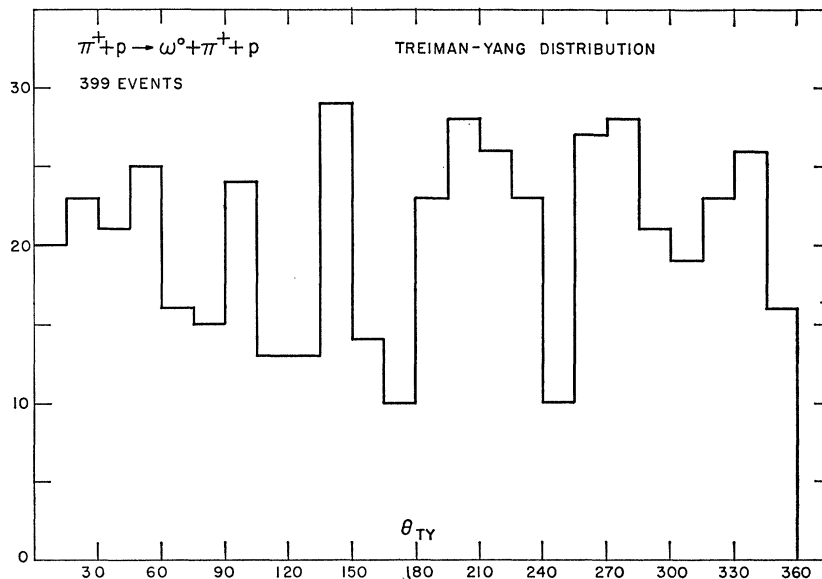

FIG. 29. Treiman-Yang angle for ω^0 produced without N^*.

[21] M. L. Stevenson, L. W. Alvarez, B. C. Maglić, A. H. Rosenfeld, Phys. Rev. **125**, 687 (1962).
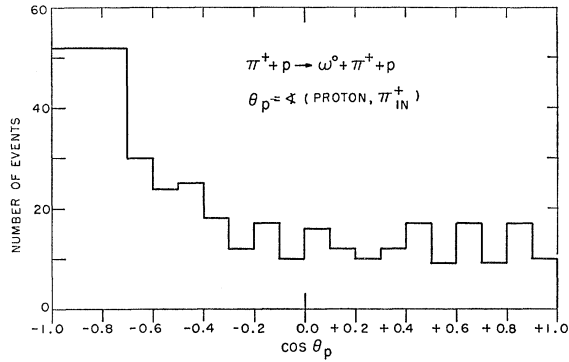[22] T. D. Lee, Phys. Rev. **139**, B1415 (1965).

FIG. 30. Production-angle distribution of the proton in ω^0 events without N^{*++}.
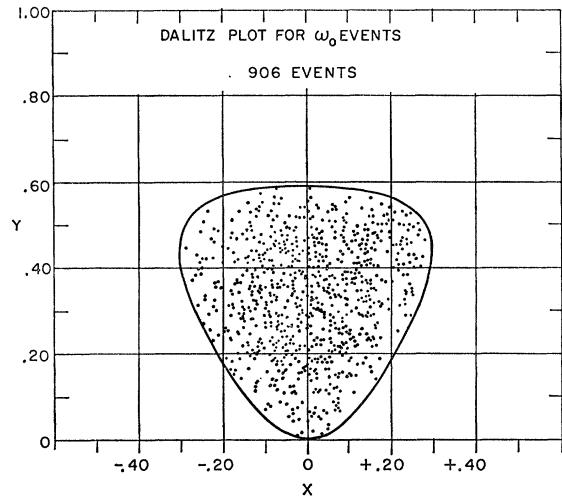

FIG. 32. Dalitz plot for ω^0 decay.

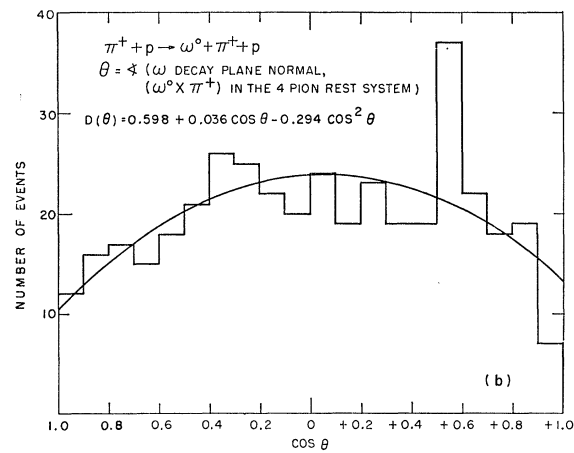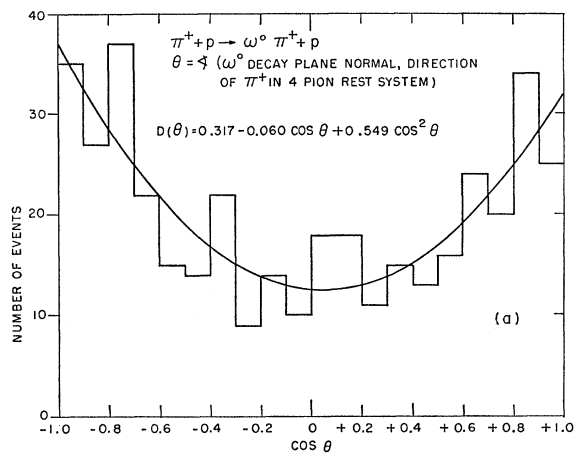FIG. 31. The ω^0-decay-plane normal distribution relative to: (a) the incident π^+ direction in the $\pi^+ + \omega^0$ rest system; (b) the direction $\pi^+_{in} \times \omega^0$ in the four-pion rest system.
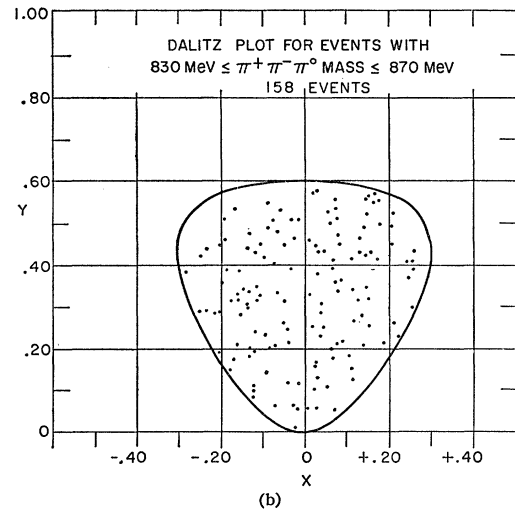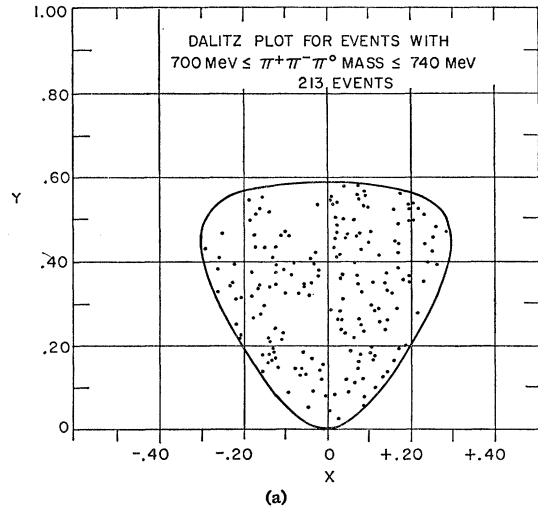

FIG. 33. Dalitz plot for two control regions: (a) 700 MeV$\leq M_{\pi^+\pi^-\pi^0} \leq$740 MeV; (b) 830 MeV$\leq M_{\pi^+\pi^-\pi^0} \leq$870 MeV.
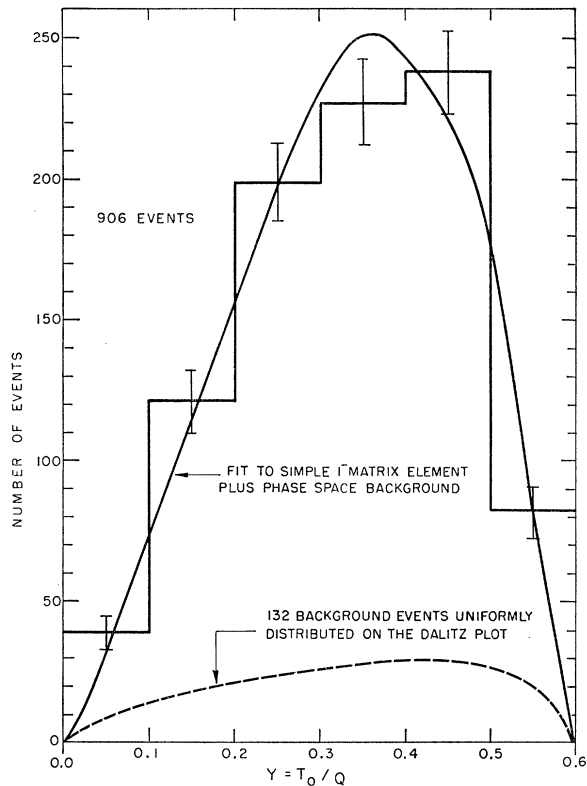
FIG. 34. A projection of Fig. 32 on to the Y axis.

tude in ω^0 decay, interfering with a C-conserving amplitude, would give rise to an asymmetry about the line $T_+ = T_-$ on the Dalitz plot. We can look for the C-violating amplitude by fitting the X distribution using odd powers of $X \equiv (T_+ - T_-)/\sqrt{3}Q$. The experimental values (Table V) of the coefficients of the odd powers of X are consistent with zero, indicating that to the accuracy of this experiment there is no observable effect of C violation in ω^0 decay.

The existence of a rapid decay $\omega^0 \rightarrow \pi^+ + \pi^-$ has been suggested by several authors.[23] We have looked for

TABLE V. Experimental values of the coefficients of X.

$$P(X) = A_0 + A_1 X + A_2 X^2 + A_3 X^3 + A_4 X^4$$

$A_0 =$	1.00 ± 0.36
$A_1 =$	0.34 ± 0.28
$A_2 =$	-19.66 ± 2.51
$A_3 =$	-2.70 ± 4.69
$A_4 =$	99.81 ± 31.31

[23] Theoretical arguments for this mode have been advanced among others by S. Glashow, Phys. Rev. Letters **7**, 469 (1961); and G. Feinberg, *ibid.* **8**, 151 (1962). Experimentally, the situation has been investigated by W. J. Fickinger *et al.*, Phys. Rev. Letters **10**, 457 (1963); W. Walker *et al.*, *ibid.* **8**, 208 (1964); S. M. Flatte *et al.*, *ibid.* **14**, 1095 (1965), who report observation of the mode $\omega^0 \rightarrow \pi^+ + \pi^-$. A compilation of G. Lütjens and J. Steinberger, *ibid.* **12**, 517 (1964) containing some of the data cited above and much other data finds no evidence for the existence of $\omega^0 \rightarrow \pi^+ + \pi^-$ and finds $\Gamma(\omega \rightarrow \pi^+ + \pi^-)/\Gamma(\omega \rightarrow \pi^+ + \pi^- + \pi^0) < 0.8 \times 10^{-2}$ with 90% confidence.

evidence of this decay mode for the ω^0 in the $\pi^+ \pi^-$ mass spectrum from the final state $\pi^+ p \pi^+ \pi^-$. The amplitude M for the reaction $\pi^+ + p \rightarrow \pi^+ + p + \pi^+ + \pi^-$ can be written as

$$M \propto A_1 + \frac{A_\omega \sqrt{\Gamma_2}}{(m - m_\omega) - i\Gamma_T/2},$$

where A_ω is the amplitude for producing an ω^0, Γ_T is the total ω^0 width, Γ_2 the partial width for ω^0 decay into $\pi^+ \pi^-$, and A_1 is the amplitude for all other processes (i.e., not involving ω^0 production) leading to the final state $\pi^+ p \pi^+ \pi^-$. The number of $\pi^+ \pi^-$ pairs observed at a given value of $\pi^+ \pi^-$ mass m_0 is the integral over all momenta and the average over spin of $|M|^2$, subject to the constraint that $(E_+ + E_-)^2 - (\mathbf{p}_+ + \mathbf{p}_-)^2 = m_0^2$. As a result of the integration, we do not expect that there will be an effect on the mass spectrum due to the interference between A_1 and A_ω. In this case, the number of $\pi^+ \pi^-$ pairs in the ω^0 region above that due to $|A_1|^2$ (which consists of phase space and ρ^0 production) divided by the number of ω^0 decaying into $\pi^+ \pi^- \pi^0$ gives Γ_2/Γ_3, where Γ_3 is the partial width for ω^0 decay into $\pi^+ \pi^- \pi^0$. Experimentally, we find $\Gamma_2/\Gamma_3 = (-2 \pm 15)/(744 \pm 29)$. This corresponds to an upper limit $\Gamma_2/\Gamma_3 \leq 0.02$.

VIII. PRODUCTION AND DECAY OF THE η^0

The absence of any production of charged η mesons in $\pi^+ p$ interactions and the observation of η^0 requires that the η have isotopic spin zero. If the decay of the η^0 into $\pi^+ \pi^- \pi^0$ conserved isotopic spin, the six sectors on the Dalitz plot would have to be equally populated.[24] The experimental distribution (Fig. 35) shows the well-established depletion of events for large T_0 and is
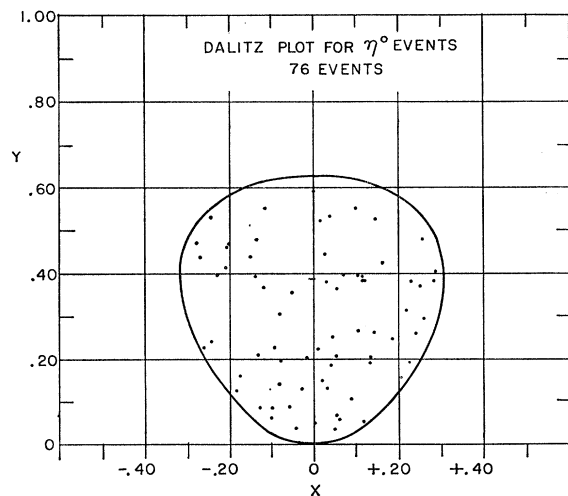

FIG. 35. Dalitz plot for η^0 decay.

[24] P. L. Bastien, J. P. Berge, O. I. Dahl, M. Ferro-Luzzi, D. H. Miller, J. J. Murray, A. H. Rosenfeld, and M. B. Watson, Phys. Rev. Letters **8**, 114 (1962).
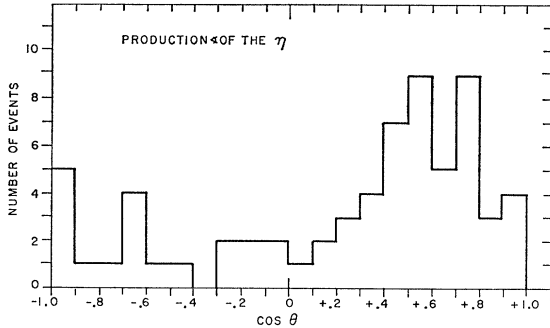
FIG. 36. Production angle of the η^0.

FIG. 37. π^+p mass spectrum recoiling against an η^0.

consistent with the 0^- assignment for the η^0.[25] The statistics are too meager to conclude anything meaningful about C violation in η^0 decay.

Production of the η^0 cannot proceed via the exchange of one pion (because of parity conservation), or two pions (because of G conservation). The simplest exchange mechanism is the $T=1$ system of three pions. Thus, there is no obvious peripheral mechanism for η^0 production. The η^0 production angular distribution (Fig. 36) is much broader than the ρ^0 or ω^0 distribution for which peripheral mechanisms do exist.

The π^+p mass spectrum recoiling against the η^0 (Fig. 37) suggests that the η^0 is produced with the $(\frac{3}{2},\frac{3}{2})$ isobar.

An upper limit of 10 MeV for the width of the η^0 can be set by this experiment.[1]

IX. CONCLUSIONS

The π^++p initial state reacts at these energies principally to excite multipion resonances. Simultaneous to the excitation of the pion system the proton is excited so that it forms the $(\frac{3}{2},\frac{3}{2})$ isobar with $T_z=\frac{3}{2}$. The low momentum transfer to the recoiling nucleon system in the production of these resonances suggests single-particle exchange as the dominant production mecha-

nism. There is, however, no known particle that could be exchanged which would be able to explain the angular distributions in ρ, ω, or N^* decay. This suggests that, as has been already noted in other experiments,[26] absorptive effects are important in understanding the decay correlations.

ACKNOWLEDGMENTS

[25] M. Chretien, F. Bulos, H. R. Crouch, Jr., R. E. Lanou, Jr., J. T. Massimo, A. M. Shapiro, J. A. Averell, C. A. Bordner, Jr., A. E. Brenner, D. R. Firth, M. E. Law, E. E. Ronat, K. Strauch, J. C. Street, J. J. Szymanski, A. Weinberg, B. Nelson, I. A. Pless, L. Rosenson, G. A. Salandin, R. K. Yamamoto, L. Guerriero, and F. Waldner, Phys. Rev. Letters 9, 127 (1963).
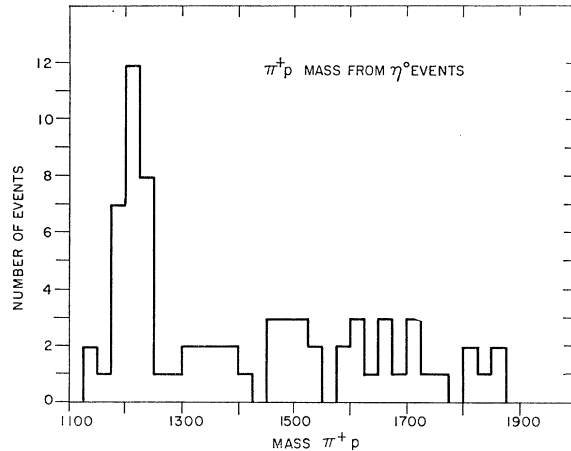
[26] For the relevant experiments see Ref. 20 above.